POLITECNICO DI TORINO

Master's Degree in Physics of Complex Systems

Master's Degree Thesis

Interplay of health interventions in time-varying contact networks

Supervisors

Prof. Luca DALL'ASTA

Prof. Nicolò GOZZI

Candidate

Cristiano MARINELLI

July 2024

Abstract

Throughout history, humanity has recurrently faced epidemics of infectious diseases, which have spread both within and between populations. From ancient pandemics like the Antonine Plague to the contemporary COVID-19 pandemic, understanding and controlling the spread of diseases has always been crucial. Mathematical modeling of epidemics plays a key role in this understanding. Over the years, epidemic modeling has evolved, incorporating interdisciplinary elements, particularly from network science. Health interventions, including non-pharmaceutical measures and pharmaceutical solutions like vaccines, have historically been crucial in mitigating disease spread. During the COVID-19 pandemic, for example, measures such as social distancing, lockdowns, mask usage, hygiene, and vaccinations were key in controlling the virus spread.

This thesis proposes a mathematical framework to model three distinct health interventions—social distancing, mask usage, and vaccination—on activity-driven networks (ADN), a mathematical framework that models the dynamic nature of individual contacts and the heterogeneity in sociability. We studied analytically how these interventions affect epidemic thresholds using the SIR model as an example, and validated them through numerical simulations. Two mechanisms for intervention adoption were considered: random and activity-based, focusing on nodes with the most or least number of contacts. Our findings highlight that protecting the most active nodes significantly enhances mitigation strategies. Among the three interventions, vaccines showed the best results, especially when targeted at these individuals. However, vaccines are not always available at the outbreak, therefore the use of alternative interventions remain crucial. Additionally, we examine the combination of interventions. In the first case study, we simulate scenarios where essential workers cannot reduce contacts, emphasising the importance of vaccinating and protecting these individuals. In the second case, we explore how the overlap in groups adopting interventions affects their effectiveness, showing that distributed adoption across the population leads to better results. Overall, this thesis combines mathematical evaluation and the interplay of health interventions in an activity-driven, time-varying network, enhancing the effectiveness of epidemic control strategies.

Table of Contents

List of Figures

Chapter 1

Introduction

Throughout its history, humanity has recurrently faced epidemics of infectious diseases, spreading both within and between populations. From ancient pandemics like the Antonine Plague, also known as Galen's Plague (165 AD-180 AD) [1], which decimated the Roman Empire and significantly impacted its society, potentially hastening its decline[2], to the contemporary COVID-19 pandemic caused by SARS-CoV-2. In this context, studying and modeling epidemics from a mathematical standpoint is crucial, as it helps us control their spread and limit their impact on our societies.

Since the introduction of the SIR model in 1917[3], there has been a continuous effort to mathematically model epidemics. The SIR model is a type of compartmental model, with SIR standing for Susceptible, Infected, and Recovered (or Removed). Over the years, epidemic modeling has evolved significantly, becoming an interdisciplinary field that incorporates elements from various disciplines, especially network science[4].

In the late 1990s, a study conducted between Stockholm University and Boston University aimed to reconstruct the network of sexual partners during the AIDS epidemic in Northern Europe [5]. This study showed that the distribution of contacts in the network followed a power law distribution. Here *power law*, or *scale-free* feature, means that the relationship in the population distribution of contacts is consistent across scales. For instance, for every four people who meet four others, there is one who meets eight, and this pattern holds true at larger scales as well. Scale invariance results in a heavy-tailed probability distribution, where rare *events* have a non-zero probability of occurring. The difference in network topology is significant; Pastor-Satorras and Vespignani [6] demonstrated that in networks with such contacts structure (i.e., degree distribution), the epidemic threshold tends to zero as the population grows. This finding marked a major shift from the approaches previously used in epidemic modeling, as networks increasingly gained a central role in epidemiology. This led to the emergence of a new subfield

known as network epidemiology.

The ultimate goals of effective epidemic modeling are to understand the mechanisms behind disease spread, predict their evolution, and propose strategies to control and mitigate them. In this context, modeling health interventions aimed at controlling disease spread is crucial. Health interventions include a range of non-pharmaceutical measures (e.g., social distancing, quarantine), behavioral changes (e.g., wearing face masks, hand hygiene), and pharmaceutical solutions such as vaccines. Historically, health interventions have played a critical role. For example, during the 2003 SARS outbreak, people adopted preventive behaviors such as wearing face masks and avoiding crowded places [7, 8, 9] . Significant behavioral reactions were also observed during the 2009 A/H1N1 influenza pandemic [10, 11], the 1918 Spanish flu pandemic[12, 13], measles [14] , and HIV [15, 16] among other diseases. During the COVID-19 pandemic, social distancing, strict lockdowns, mask usage, hygiene measures, and vaccinations were key in slowing down the spread of the new virus [17, 18, 19, 20, 21]. Therefore, it is crucial to model appropriately health interventions, determining not only which measures are implemented but also the most effective strategies for their application. This includes identifying the optimal timing, scale, and combination of interventions to maximize their impact on controlling and mitigating the an epidemic.

In this thesis, we propose a mathematical framework to model three different health interventions: social distancing, mask usage, and vaccination. These interventions are studied on a specific type of time-varying network that considers the important topological property of scale invariance: activity-driven networks (ADN)[22]. These networks evolve over time, modeling the temporal dependency of each individual's contact network, and assign an activity level to each individual. Activity is a measure of an individual's sociability within the network and is assigned based on power law distributions. Temporal dependency plays an important role as the network's mutation time is comparable to the pathogen's transmission time

More in details, in this thesis we studied how the adoption of the three health interventions affects the epidemic thresholds, first proposing an analytical solution to the problem using the SIR compartmental model, and then verifying its accuracy through numerical simulations that reproduce the described framework. We consider two mechanisms for adopting health interventions: one random, and one activity-based, where individuals who are most (or least) socially inclined decide whether to adopt the interventions. We find that, due to the topology of scale-invariant networks, individuals in the heavy tails (i.e., those with the most contacts), are key drivers in virus transmission. These individuals act as *super spreaders*, and identifying and protecting them significantly improves the effectiveness of mitigation strategies.

In the analysis of all three health interventions taken individually, different adoption

types have shown a hierarchy in terms of effectiveness in reducing spread. Random adoption performs better than adoption given to less active individuals but worse than when adoption is among the most active. Specifically, the use of face masks manages to prevent the spread of less infectious pathogens but only slows down others. Social distancing, taken to the extreme of total elimination of contacts (though unrealistic), has the potential to stop even more infectious pathogens; however, this comes with the social and economic cost of extreme isolation measures. Vaccines have consistently shown better results across all adoption types among the three interventions, especially when concentrated among super-spreaders. However, vaccines have the disadvantage of not always being available at the onset of an epidemic.

In addressing the limitations of individual health interventions, we then studied their combinations.
We focused on two specific case studies to investigate the interplay of health interventions. In the first case study, we simulated a scenario where individuals with more contacts cannot limit their social activity even during a lockdown, as they are essential for the basic needs of the population, such as healthcare workers and those involved in the transportation and distribution of goods. We quantified the effects of the other two health interventions (mask usage and vaccination) applied to these individuals to compensate for their inability to reduce contacts, and we identified the most effective strategies, confirming the higher effectiveness of vaccination. This finding highlights the importance of protecting essential workers, or more generally, individuals who cannot reduce their contacts, in contexts like the COVID-19 pandemic. Prioritizing these individuals in the vaccination rollout and providing them with personal protective equipment is crucial for their safety, overall public health, and effective epidemic control.

In the second case study, we evaluated how the combined effectiveness of two interventions changes as the overlap between the groups adopting them increases. Indeed, during the COVID-19 pandemic, we observed that many individuals adopted a range of protective measures, while others did not protect themselves at all. This phenomenon is due to the multifaceted nature of health intervention adoption, which is influenced by personal beliefs, exposure to information, personal experiences, and several other factors. To achieve this, we assigned two health interventions to two different groups of individuals. The groups ranged from being completely disjoint to having varying levels of overlap, up to the scenario where one group applied both health interventions while the other applied none. The simulations show that the response improves as the number of adopting individuals increases, i.e. as the overlap decreases. Although the number of health interventions remains constant, distribution across the population leads to better results.

We structured the thesis as follows:

In the second chapter, we discuss the cornerstone of epidemic modeling, namely

compartmental models, how they can be used to describe pathogen transmission, and evaluate epidemic thresholds under the assumption of homogeneous mixing of network nodes, introducing some fundamental quantities for epidemic description.

In the third chapter, we first introduce the heterogeneous mixing. We then present time-varying activity-driven networks, how to model epidemic processes on them, and evaluate thresholds first without any health interventions and then with social distancing, replicating results obtained in previous studies. We solve the problem analytically for random adoption by individuals and activity-dependent adoption, using these methods as the basis for modeling the other two health interventions.

The results are then divided into two chapters. In the fourth chapter, we present the modeling of mask usage in the proposed framework, showing the solutions to the problem and validating thresholds for both random and activity-dependent adoption. We then introduce vaccinations and show the analytical solution for the combination of all three health interventions under random adoption.

In chapter five, we present the two case studies. In the first, we analyze a scenario where the majority of the population below a certain activity threshold limits their interactions by applying social distancing, while those above the threshold may receive or not a vaccine. We simulate and compare the effects of different adoption levels by the more active individuals while keeping conditions for the less active constant. We repeat these simulations replacing vaccination with mask usage and considering the possibility of inconsistent mask usage. We then evaluate the percentage reduction in infection peaks and the final fraction of total infections, comparing the results of the three combinations.

In the second part, we introduce a new parameter describing the overlap of two health interventions in population adoption. We analyze two combinations of health interventions: vaccines/social distancing and vaccines/mask usage. For both cases, we simulate different combinations of adoption and overlap, and finally, evaluate the percentage reduction in infection peaks and total infections.

The final chapter summarizes the results and outlines potential future work, such as relaxing further approximations, comparing with empirical data, and introducing feedback loop between epidemic and behavior. The appendices provide detailed descriptions of the algorithmic methods developed in the programming language *Julia* for this thesis, offering a comprehensive overview of the technical aspects of the research.

Chapter 2

Modeling epidemics

2.1 Compartmental models in epidemiology

First studies describing the dynamics of epidemics through compartmental models were published in 1916-17 by Ross and Hudson [3], and in 1927 by Kermack and McKendrick[23].
The aim of compartments is to contain the individuals of a population at different stages of contagion that can be experienced during the spreading of an epidemic. One of the most simple compartmental models is organized as follow:

- **Susceptible** compartment contains the healthy individuals who may be infected;

- **Infected** compartment contains the infected individuals who can transmit the disease to the susceptibles;

- **Recovered** (or **Removed)** compartment contains the individuals who healed from the disease and can no longer be infected.

The compartmental structure usually gives the name to the model under study. Therefore, the one just described is generally referred to as the **SIR model** from the initial letters of the compartments (Susceptible-Infected-Recovered).

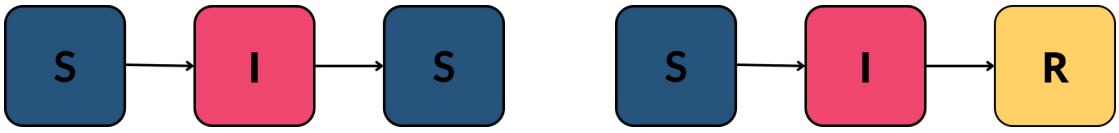

(a) SIS scheme **(b)** SIR scheme

Figure 2.1: Schemes of Compartmental models. In 2.1a, the scheme of the SIS model is shown, where infected individuals become susceptible to the disease again after recovering. In 2.1b, the scheme of the SIR model is shown, where infected individuals transition to a recovered state and cannot be infected again.

Other compartments can be introduced, for example for the deceased (D), the vaccinated (V), and for people in a latent state (or exposed, E), and also different compartments for two or more competing disease can be used. The combination of compartments and the tuning of the transition rates can give birth to an infinite spectrum of models (as in the figure from article *Abrams et al.* [24]) representing different populations and different pathogens.

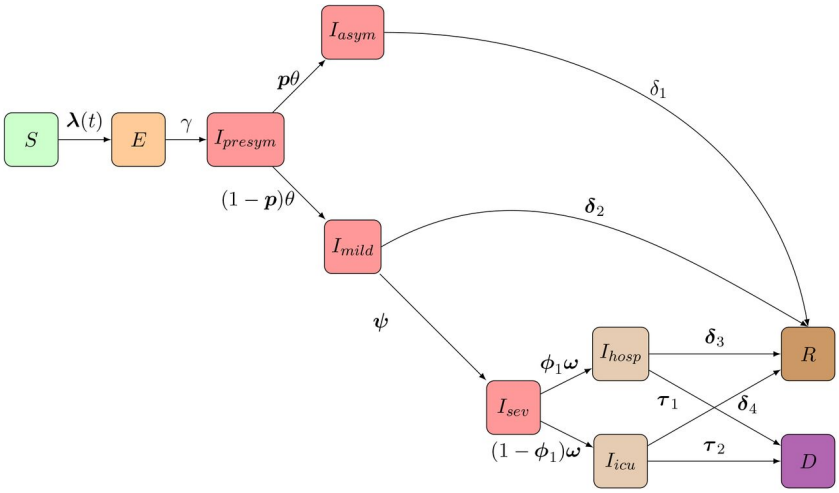

Figure 2.2: compartmental model proposed for early phase of the Belgian COVID-19 epidemic [24]

The total population in general is a function of time $N(t)$, and the sum of the populations inside the compartments has to respect the constraint to be equal to the total population $N(t)$. The population is considered constant if births and deaths are excluded from the model, loosing time dependence $N(t) \equiv N$.
The number of individuals inside of a compartment are time dependent and are labelled with capital letters, $S(t)$, $I(t)$, $R(t)$. The population density of a

compartment is indicated with the corresponding lowercase letter and it is equal to the compartment population divided by N

$$s(t) = \frac{S(t)}{N} \quad i(t) = \frac{I(t}{N} \quad r(t) = \frac{R(t)}{N} \tag{2.1}$$

and the constraint becomes $s(t) + i(t) + r(t) = 1$.
Individuals can flow from a compartment to the other according to transition rates and interaction. In compartmental models the transitions, in general, are of two elementary types:

- **spontaneous transition** of an individual from a compartment to another. Examples are the healing of an infected ($I \to R$) or the passage from a latent to an infectious condition in the SEIR model ($E \to I$);
- transitions involving **interactions** of individuals of two different compartments. This is the case of susceptibles that, interacting with infected become infectious themselves in the SIR model ($S + I \to 2\,I$).

Transitions of the first type are ruled by a transition rate only (i.e., recovery rate). The second type process depends on a rate, but also on the topology of contacts between individuals of different compartments. The simplest possible approximation for the contacts between compartments is the homogeneous mixing, in which the probability of interaction is directly proportional to the product of the two individual density involved in the process. The constant characterizing the proportionality is k, in the next chapter it will be called the average degree of the network, and it indicates how many other people an individual will meet on average during the unit of time.

The transition of the individuals between the compartments can be seen as a flow. Let's consider the SIR model as an example. Focusing on the I compartment it presents an inflow that is a transition of the second type described, and an outflow of the second type. The inflow is characterized by the infection rate called λ and average degree k, the outflow by the recovery rate μ. In the literature, the product of λ and k is usually referred as β. In the development of this thesis the two variables will be left separate. Defined all these elements it is possible to write the equation for the discrete time evolution of the population density of the compartment:

$$i(t + \Delta t) = \lambda k s(t) i(t) \Delta t - \mu i(t) \Delta t \tag{2.2}$$

In these conditions it is possible to write the equations for each compartment. To show the treatment of these equations and what are the solutions, in the next section we focus on the specific example of the SIR model without death and births, which will be used as a basis for the rest of the thesis.

2.2 SIR model

As mentioned before, the SIR model is one of the most famous compartmental models and its simplicity makes it a good candidate to explore the interplay of health intervention. Before introducing the complexity of our approach, we briefly review the dynamics with homogeneous mixing, starting with the system of differential equations describing the evolution of the number of individuals in each compartment.

$$\begin{aligned} \frac{ds(t)}{dt} &= - s(t)i(t)k\lambda \\ \frac{di(t)}{dt} &= s(t)i(t)k\lambda - \mu i(t) \\ \frac{dr(t)}{dt} &= \mu i(t) \end{aligned} \tag{2.3}$$

where it has been possible to take the continuous limit taking into account the time steps to be small and the thermodynamic limit for the total population $N \infty$. At early stages it is possible to make other two assumptions useful for the solution of the differential equations. First assumption is $I(0) \ll N \rightarrow i(0) \ll 1$, meaning that we have a little number of infected at the beginning of the outbreak. The second is that at the beginning the R compartment is almost empty, i.e., very few individuals recovered from the disease. Joining this with the previous approximation brings to $S(t) = N - I(t) \approx N \rightarrow s(t) \approx 1$, meaning that almost all the population is in the Susceptible compartment. These conditions take the name of **early stage approximation**. The ODE system becomes under this approximation:

$$\begin{aligned} \frac{ds(t)}{dt} &= - [1 - i(t) - r(t)]ki(t)\lambda \approx i(t)k\lambda \\ \frac{di(t)}{dt} &= [1 - i(t) - r(t)]ki(t)\beta - \mu i(t) \approx i(t)(k\lambda - \mu) \\ \frac{dr(t)}{dt} &= \mu i(t) \end{aligned} \tag{2.4}$$

The solution for $i(t)$ is an exponential function of the form:

$$i(t) \approx i(0)e^{t(k\lambda - \mu)} \tag{2.5}$$

Looking at a typical plot of the dynamics of compartments in Fig. 2.3, this solution refers to the early stage, highlighted in grey. The solution for $i(t)$ can grow and become an outbreak only if the sign of the exponential is greater than zero. This suggests the definition of the fundamental quantity R_0:

$$R_0 = \frac{k\lambda}{\mu} \tag{2.6}$$

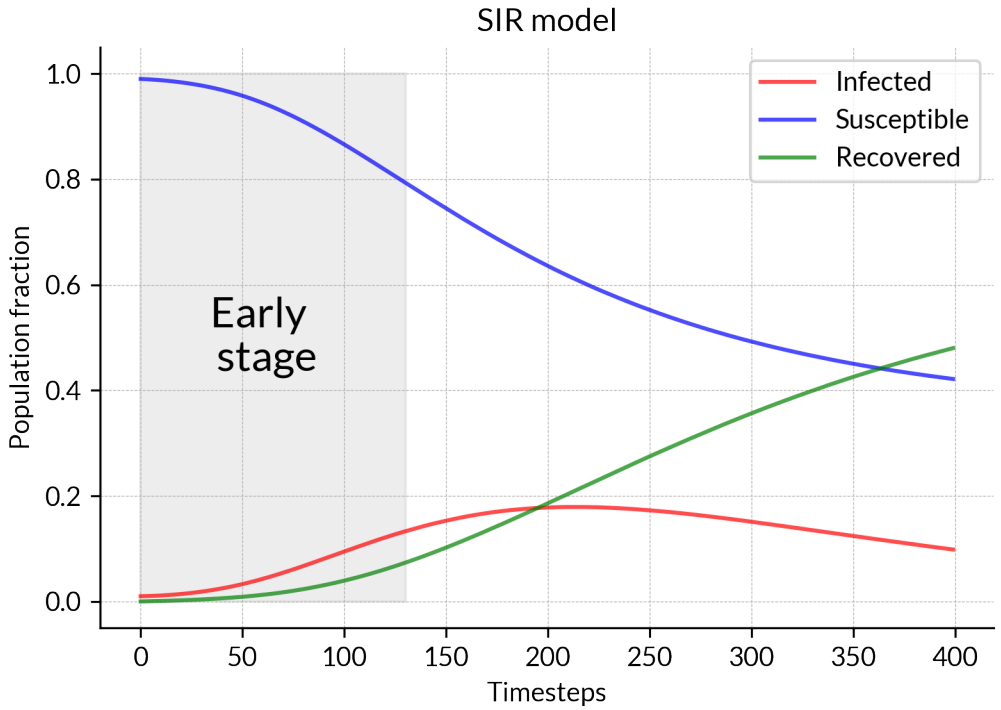

Figure 2.3: Compartment dynamics for SIR model highlighting the early stage of the contagion. In early stage the approximation $N \approx S(t)$ and the dynamics of compartments is described by (2.3)

R_0 is called the basic reproduction number of the infection and it is the expected number of secondary new cases generated by an infected individual in a population infinitely susceptible, as in the early stage approximation. The condition, in this model, for the disease to spread becomes $R_0 > 1$, only when $\lambda k > \mu$.

Chapter 3

Social Networks

3.1 Time-varying activity based social network model

In the previous chapter the theme of network has intentionally not received the attention it deserves. To keep equation easy it has been only mentioned in the presentation of k, the average degree of the network. Up to now homogeneous mixing hypothesis has been used, but many observed real social networks exhibit a very heterogeneous topology [25, 22, 26].
The word average, suggests the presence of distributions. In fact, homogeneous mixing can be interpreted as a system with a distribution of the connections among the nodes heavily peaked around the average, with variance tending to zero, making $k \approx \langle k \rangle$ a good first approximation. Empirical evidence shown many epidemiological networks to be heavy-tailed distributed, with variances different from zero and the existence of nodes with a really high number of connection. This makes the average not a good variable for the study of spreading anymore. To intuitively justify the last sentence, let take the Latin proverb *Omnes viae Romam ducunt*, translated as "all roads lead to Rome". The rise of the Roman Empire fuelled the development of a dense network of roads connecting Rome to the vast empire. If a traveler, during the empire, starting from his city (a node), would choose the street to take (link) randomly, and after reaching the new city choose the new direction again randomly, at each steps is more likely to be nearer to Rome. Mathematically can be shown that the probability of reaching a node is directly proportional to its degree [27], again interpretable as the more connected you are, the easier it is to find you. Making a little transformation calling the cities as individuals, the roads as their interactions, and the traveler as a virus, the more sociable individuals will be easily reached, and being heavily connected become a so called "super-spreader" [28]. The fluctuations of the degree distribution start to

play the main role in the dynamic of the spreading properties.
Up to now the networks were static in time. In some real networks the dynamic processes evolve much faster than the topology, this is the example of internet, were a virus can spread in a network almost static. This is not the case of human interactions were social contacts happen at the same time scale of disease spreading. So, a more realistic representation is a network that varies in time. Another limit of the static network is the fact that a node with a certain degree will always have that degree, but human interact in different way depending on their personalities, situations and many other factors. The idea here is to represent this variability assigning to every node an *activity potential*. The activity potential is, to some extent, a measure of sociability of a person: the higher the activity potential, the more likely the node will create links. The activity potential a is a probability rate and its distribution has been empirically measured from three different dataset in Ref. [22]: the collaborations "Physical Review Letters", the messages on Twitter, and costarring in cinema recorded on Internet Movie Database (IMDb). The results show heterogeneity in the activity, confirming again the necessity of relaxation of the homogeneous approximation.
Based on these observations, Ref. [22] has proposed a new model to represent the time-varying nature of contacts, named the activity driven model. Before explaining how it works, we introduce all its fundamental parameters and ingredients. First of all, N is the number of nodes. The probability distribution of the activity potential chosen is a power law, whose boundaries are $\epsilon < a < 1$, and the exponent is α. The left boundary is chosen in order to avoid future divergences in the calculation. The distribution takes the form:

$$P(a) = \frac{1-\alpha}{1-\epsilon^{1-\alpha}} a^{-\alpha} \tag{3.1}$$

and the activity are assigned to the nodes through the inverse transform sampling (see Appendix A for more details).
Another parameter is Δt, the time step in which the network changes. Each node has the possibility to create m nodes at each time step.
Once all the parameters are presented, the time evolution of the network in the model is generated through the iteration of this sequence of steps:

- At each time step t the network starts with N completely disconnected nodes;
- Each of the nodes i has a probability $a_i \Delta t$ to become active and randomly generate m links connecting to m other vertices. Non-active nodes are not necessarily isolated, can still receive connections from active nodes;
- At the next time step $t + \Delta t$ all the edges in the network are deleted, going back to the situation with all isolated vertices. From this sequence follows that every interaction has a constant duration of Δt

The model just proposed is random because of the way the link are selected and Markovian because deleting the edges there is no way for the nodes to have memory of the previous time steps. The dynamic of the network is fully encoded in the activity distribution $F(a)$.

3.2 SIR model on activity driven networks

Studying the dynamic of the outbreak, one can sum the contacts of every time step, generating an aggregate static network. The results for epidemic thresholds from the previous section are not valid for this aggregate network, this because at some time a node could not be active and do not spread the disease. In fact in this framework, the infected node can only attempt the contagion before the elimination of the nodes at the end of the time step, while the recovery is attempted before the network of the following time step is generated.
It is possible to more precisely quantify the epidemic threshold by working on time and activity rates. The epidemic dynamics is evaluated taking into account a mean-field approach and with the assumption that every node with the same activity behave in a statistical similar way. In this settings, we can write the system of equation describing an SIR model unfolding on activity driven networks. The belonging to a class will be indicated by a subscript, while the time in the superscript, I_a^t. The λ is the probability rate of infection between susceptible and infected, per contact, while μ is the probability rate for an infected to spontaneously recover and pass to the R compartment.
As always the threshold is defined by the solution of the equation for the I compartment at early stages. Suppose at the beginning $I(0) \ll N \to I_a^t \ll N_a$ and also $R(0) = 0$, giving the approximation $S_a^t = N_a^t - I_a^t - R_a^t \approx N_a^t$, the number of infected individuals of class a at the time $t+\Delta t$ is given by (3.4). The first two term on the right-hand side of the first line equation are pretty standard representing the infected in the a class at previous time and the recovered at previous time. The third term represent the interaction between an activated susceptible and all the possible infected, in fact the infected is inside the integral that spans over all the distribution. The fourth term is the case in which the active one is one of the infected of the network, regardless of his activity class, and the susceptible is receiving a link, in fact in this term the activity a appear inside the integral.

$$I_a^{t+\Delta t} = I_a^t - \mu \Delta t I_a^t + \lambda m \Delta t a S_a^t \int da \frac{I_a^t}{N} + \lambda m \Delta t S_a^t \int da \frac{a I_a^t}{N} \tag{3.2}$$

Applying the early stage approximation $S_a^t \approx N_a$

$$I_a^{t+\Delta t} = I_a^t - \mu \Delta t I_a^t + \lambda m \Delta t a N_a \int da \frac{I_a^t}{N} + \lambda m \Delta t N_a \int da \frac{a I_a^t}{N} \tag{3.3}$$

Only terms involving an interaction with S_a^t are relevant, because can transform to element of $I_a^{t+\Delta t}$ at the next time step. In the second line is applied the early stage approximation. In order to evaluate the total sum of infected, and being $F(a)$ a continuous distribution, integrals over the spectrum of a are applied on both sides of the equation:

$$\begin{aligned}\int da I_a^{t+\Delta t} = \int da I_a^t - \mu\Delta t \int da I_a^t + \lambda m \Delta t \int da a N_a^t \int da' \frac{I_{a'}^t}{N} + \\ + \lambda m \Delta t \int da N_a^t \int da' \frac{a I_{a'}^t}{N} \end{aligned} \tag{3.4}$$

$$= I^t - \mu\Delta t I^t + \lambda m \Delta t \langle a \rangle I^t + \lambda m \Delta t \Theta^t \tag{3.5}$$

with Θ^t having the form

$$\Theta^t = \int da' \frac{a I_{a'}^t}{N} \tag{3.6}$$

and interpretable as the mean field probability of an infected to activate and meet a susceptible.
The subscript a is now absent because the integral give the whole I compartment. The average come from the integral noticing that the N at the denominator do not depend on a' and $\frac{N_a^t}{N} = F(a)$ being the activity distribution.
Bringing the I^t term on the lefthand side, dividing by Δt and taking the continuous time limit

$$\partial_t I^t = -\mu I^t + \lambda m \langle a \rangle I^t + \lambda m \Theta^t \tag{3.7}$$

Another equation is needed to find the solution. Looking at the expression of Θ, it suggest the creation of another equation multiplying by a both sides of (3.3) and then again integrating over a

$$\begin{aligned}\int da\, a I_a^{t+\Delta t} = \int da\, a I_a^t - \mu\Delta t \int da\, a I_a^t + \lambda m \Delta t \int da\, a^2 N_a^t \int da' \frac{I_{a'}^t}{N} + \\ + \lambda m \Delta t \int da\, a N_a^t \int da' \frac{a I_{a'}^t}{N} \end{aligned} \tag{3.8}$$

$$\Theta^{t+\Delta t} = \Theta^t - \mu\Delta t \Theta^t + \lambda m \Delta t \left\langle a^2 \right\rangle I^t + \lambda m \Delta t \langle a \rangle \Theta^t \tag{3.9}$$

Repeating the same process as for the equation in I the differential equation is

obtained also for Θ

$$\partial_t \Theta^t = -\mu\Theta^t + \lambda m \left\langle a^2 \right\rangle I^t + \lambda m \langle a \rangle \Theta^t \tag{3.10}$$

The two differential equations lead to a system that can be written in Jacobi matrix form as

$$\begin{bmatrix} \partial_t I^t \\ \partial_t \Theta^t \end{bmatrix} = \begin{bmatrix} -\mu + \lambda m \langle a \rangle & \lambda m \\ \lambda m \langle a^2 \rangle & -\mu + \lambda m \langle a \rangle \end{bmatrix} \begin{bmatrix} I^t \\ \Theta^t \end{bmatrix} \tag{3.11}$$

The solutions are a linear combination of two exponentials in time multiplied by the eigenvalue of the matrix, so the greater of the two is the one leading the trend of the function. In this way, a pandemic can spread only if the bigger eigenvalue is greater than 0. To find the the eigenvalue solve the eigenvalue equation

$$det(J - \mathbb{I}\Lambda) = 0 \tag{3.12}$$

$$det\left(\frac{J + \mathbb{I}\mu}{\lambda m} - \frac{\Lambda - \mu}{\lambda m}\right) = 0 \tag{3.13}$$

$$det(J' - \Lambda') = 0 \tag{3.14}$$

with

$$J' = \begin{bmatrix} \langle a \rangle & 1 \\ \langle a^2 \rangle & \langle a \rangle \end{bmatrix} \tag{3.15}$$

and

$$\Lambda' = \frac{\Lambda - \mu}{\lambda m} \tag{3.16}$$

The transformation is not strictly necessary but simplify the calculation when the health intervention are introduced. In this case the solution of (3.14) is

$$(\langle a \rangle - \Lambda')^2 - \left\langle a^2 \right\rangle = 0 \tag{3.17}$$

$$\Lambda'^2 - 2 \langle a \rangle \Lambda' + \left(\langle a \rangle^2 - \left\langle a^2 \right\rangle \right) = 0 \tag{3.18}$$

$$\Lambda'_{(+,-)} = \langle a \rangle \pm \sqrt{\langle a^2 \rangle} \tag{3.19}$$

$$\Lambda_{(+,-)} = -\mu + \lambda m \left(\langle a \rangle \pm \sqrt{\langle a^2 \rangle} \right) \tag{3.20}$$

remembering the condition $\Lambda_+ > 0$

$$-\mu + \lambda m(\langle a \rangle + \sqrt{\langle a^2 \rangle}) > 0 \tag{3.21}$$

$$\frac{\lambda}{\mu} > \frac{1}{m(\langle a \rangle + \sqrt{\langle a^2 \rangle})} \tag{3.22}$$

$$R_0 = \frac{\lambda}{\mu} m(\langle a \rangle + \sqrt{\langle a^2 \rangle}) > 1 \tag{3.23}$$

A first easy approach to verify the validity of this threshold is to see it has as limiting case the homogeneous mixing approximation. Remember it is characterized by a narrow distribution peaked around the average degree. In this case the homogeneous mixing can be reached if all the vertices have $a \approx 1$, a narrow distribution for a peaked around 1, with $\langle a \rangle = 1$ and $\langle a^2 \rangle = 1$. The expression for the threshold become $R_0 = \frac{\lambda}{\mu} 2m$. At every time step all the nodes generate m edges causing the average degree to be equal to $\langle k \rangle = 2m$, making this expression equal to the one found for the homogeneous mixing in (2.6).
This is not a good validation, first of all because it is only valid for a limiting case, but also because although the m partner are chosen randomly at each time step, the odds of the presence of a node that receives multiple links also in a few time steps is not zero.

To validate the threshold then, we use simulations. The algorithm simulates the progression at each time step in the SIR activity-driven, time-varying network. The Julia programming language have been chosen being a good compromise between high performance running speed and developing time. The simulation models a large population of $N = 10^5$, starting with a small percentage of infected nodes ($i(0) = 1\%$). The model runs until there are no infected individuals remaining in the population. The parameters are chosen, and the simulation is repeated 100 times. Then, only the λ parameter is changed, and the 100 simulations are repeated. The initial λ is set to 0, resulting in $R_0 = 0$, which does not break the threshold. Successive λ values are selected such that some are expected to be below the epidemic threshold and some above it. At the end of every simulation the total fraction of recovered is saved. This number indicated with r_∞, indirectly tell if the outbreak has spread or not. In 3.1, a plot of the average value of r_∞ versus λ shows a phase transition around the $R_0 = 1$ value. It is important to note that each point on the plot represents a different disease. Diseases characterized by values of $R_0 < 1$ show a mean value of r_∞ tending to zero, around the value $R_0 = 1$ starts to grow, and for large values of R_0 the epidemics effectively affects the population, and are more likely to spread. The figure shows two axes: one with λ values (upper) and the other with corresponding R_0 values (lower) derived using (3.23). Although the R_0 plot better emphasizes the phase transition around the value of 1, we chose to only plot λ during our simulations. This approach allows us to compare the same diseases experiencing different health intervention strategies on the same abscissa. This will become more evident in the next sections. The combination of parameters used in the simulation has the goal of making possible that the $R_0 = 1$ condition is verified for values of $\lambda < 1$.

Another statistical variable that emphasizes the phase transition is the variance of r_∞. Specifically, around the phase transition, a maximum in the threshold value is observed. Intuitively, at small λ values, the pandemic never starts, and at larger

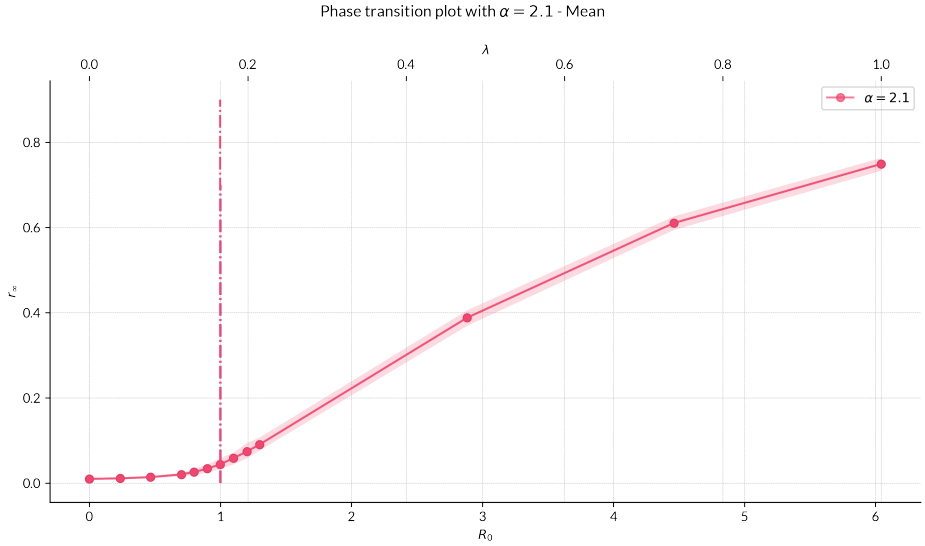

Figure 3.1: Phase transition plot of r_∞. The plot displays the final epidemic size ($r_\infty = R_\infty/N$) with 95% confidence intervals for different values of λ. Values of λ are indicate in the above x-axis with the corresponding R_0 value below. Vertical dashed line indicates the analytical threshold derived from (3.23). Results are obtained by 10^2 stochastic simulation for each point and with the following model parameters: $\mu = 10^{-2}$, $N = 10^5$, $m = 2$, $i_0 = I_0/N = 0.01$ (initial fraction of infected seeds), while for the power law distribution the minimum value $\epsilon = 10^{-3}$, maximum equal to 1, and characteristic power $\alpha = 2.1$

values, it always spreads. Around the threshold, some simulations result in a spread while others do not, causing the variance of r_∞ to increase. In the plot in 3.2, the variable used is the normalized relative variance $\sigma_{r_\infty}/\sigma_{r_\infty}^{max}$, ensuring that the y-axis scale always ranges between 0 and 1. Its maximum is around the threshold value analytically predicted, confirming the presence of a phase transition.

In the next section we modify the framework just defined to show how we can introduce health interventions.

3.3 Health interventions

Two parameters λ and μ summarise the biological features of a disease in the mathematical model, but the spreading is not only influenced by these. The health intervention can be also modelled with the aim of slowing down or do not even start the pandemic. Different ways of modelling health intervention exist, in this section three will be introduced being also the explored during the simulations:

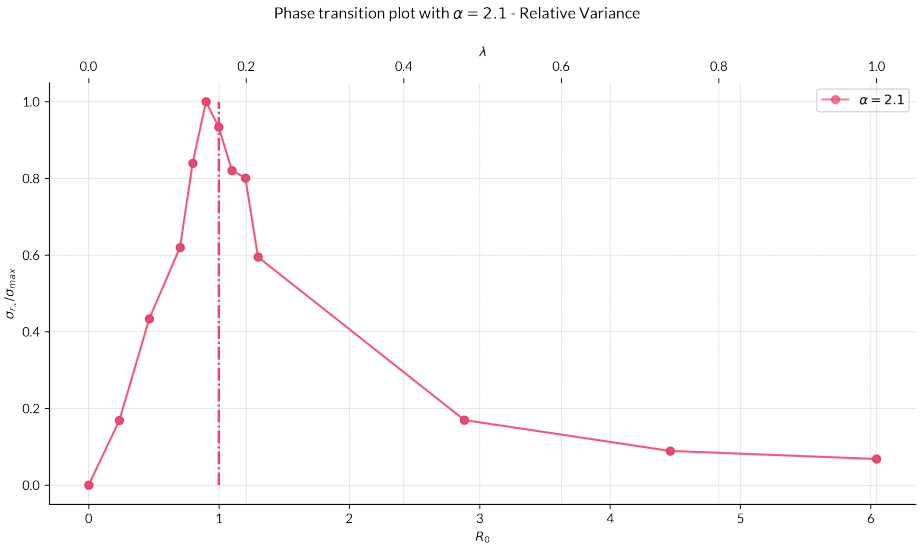

Figure 3.2: Phase transition plot for the relative variance. The plot displays the normalized relative variance $\sigma_{r_\infty}/\sigma_{r_\infty}^{max}$ for different values of lambda. The simulation data are the same of the plot in figure 3.1

- activity reduction
- use of face mask
- vaccination

Before explicit how the health intervention is modeled, another important degree of freedom has to be mentioned. We have to put a degree of freedom on who is going to adopt health interventions, also in this case three will be used:

- perfect adoption
- random adoption
- adoption based on activity

It is called perfect adoption when every individual in the model adopts the health intervention.
The random adoption introduce a number between 0 and 1, being the fraction of individual, chosen randomly, adopting the measure. There will be a fraction for each compartment, in our case w is the fraction referred to susceptible and p the one referred to infected. Notice that the perfect adoption can be seen as a the particular case with $p = w = 1$.

The adoption based on activity, is a strategy that assigns the health intervention to individuals with a activity below (or above) a certain threshold activity value. In this first approach the health intervention will be presented with perfect and random adoption condition.
The activity reduction, at this starting point affects λ indirectly, in fact we have assumed in the homogeneous mixing the probability to meet an individual from a compartment to be equal to the size of the compartment. The activity reduction can be translated in a discount factor to this probability. It is possible to give different discount to individuals of different compartments in order to simulate realistic scenarios such as infected activity reduction (γ) to be more effective than that of susceptible individuals (Ψ). The discount factor are always number between 0 and 1, and it is the more effective the more approaches zero, e.g. a reduction of 60% in activity for the infected translate in a $\gamma = 0.4$ in the model.

$$\begin{aligned} &\beta \to [w\Psi + (1-w)][p\gamma + 1 - p]\lambda \\ &perfect\ \ adoption\ \ p = w = 1 \\ &\beta \to \Psi\gamma\lambda \end{aligned} \tag{3.24}$$

The adoption of face mask affects β in a more direct way but it has similar effects on the final expression for the reduction. The face mask is modeled always as a discount factor and it reduce the probability to contract the infection during the contact. An effectiveness of the face mask of the 30% translate in the model in a $\alpha_m = 0.7$ multiplicative factor. Developing the multiplications is important to notice that the discount factor can appear with a 0, 1 or 2 exponent representing respectively if none uses face mask, only one of the two individuals uses it, and if both use the face mask. In this case the fraction of adopters are r_s for susceptibles and r_i for infected and the expression for beta modifies in this way

$$\begin{aligned} &\beta \to [r_s\alpha_m + (1-r_s)][r_i\alpha_m + ((1-r_i)]\lambda \\ &perfect\ \ adoption\ \ r_s = r_i = 1 \\ &\lambda \to \alpha_m^2\lambda \end{aligned} \tag{3.25}$$

Different ways of modeling the vaccination campaign have been studied during the years, using game theory ideas or introducing compartments for vaccinated. In this thesis the vaccination is a "one shot" money toss. The money tosses become two in case of random adoption. Introduce two probability, one is the probability (ρ) to get vaccinated, the other is the probability(the effectiveness of the vaccine ϕ), if vaccinated, to become immune and go directly in the R compartment (or a R_v this choice does not affect the evolution) or to stay in the original compartment. After this setup the simulation starts with. Being at the beginning the infected population small, the vaccination has a relevant impact

most of all on the susceptible compartment modifying in this way the assumption $S \approx N$ to $S \approx N - R \approx N - N\rho\phi = N(1 - \rho\phi)$. This again can be interpreted as a discount factor for β

$$\begin{aligned} &\lambda \to (1 - \rho\phi)\lambda \\ &perfect\ adoption\ \ \rho = 1 \\ &\lambda \to (1 - \phi)\lambda \end{aligned} \tag{3.26}$$

3.4 Social distancing in activity driven time-varying network

The results of this section are mainly from Ref. [29] In this paper the health intervention are also called behavioural changes and are evaluated the effects of the social distancing on the activity driven time-varying network. As written in the previous section, social distancing is modeled as a discount factor of the rate of infection, moreover the adoption can be random or based on the activity.
In this section we report the starting equation, skipping to the results for the thresholds, and show the same plot replicated with our algorithm. This part of the work has been useful to test the correct functioning of the algorithm, before proceeding with the new analysis that will be shown in the next chapter.

Starting from the random adoption, the fraction of susceptible nodes adopting the activity reduction will be indicated with w and apply a reduction of ψ, while the fraction of infected is indicated with p and the experienced reduction with γ. Remember the condition to be between zero and one values is valid for all four parameters. The equation for the infected at time step $t + \Delta t$ for the infected with activity a, this time reads at early stage

$$\begin{aligned} I_a^{t+\Delta t} = I_a^t - \mu\Delta t I_a^t + \lambda m \Delta t a S_a^t (w\psi + 1 - w) \int da \frac{I_a^t}{N} + \\ + \lambda m \Delta t S_a^t \int da (p\gamma + 1 - p) \frac{a I_a^t}{N} \end{aligned} \tag{3.27}$$

Assuming the early stage approximation $S_a^t \sim N_a^t$, obtaining:

$$I_a^{t+\Delta t} = I_a^t - \mu\Delta t I_a^t + \lambda m \Delta t a N_a^t \psi_w \int da \frac{I_a^t}{N} + \lambda m \Delta t N_a^t \gamma_p \int da \frac{a I_a^t}{N} \tag{3.28}$$

with $\psi_w = 1 - w(1 - \psi)$ and $\gamma_p = 1 - p(1 - \gamma)$.
The first two terms on the right hand side are the very same of the standard case

as in the previous section. The third term representing an active susceptible that activates and meet an infected, is now multiplied by the new factor ψ_w, and the fourth term, representing the infected node activation case presents the γ_p factor. Proceeding, the calculations are similar to those shown above and the complete discussion is given in the appendix. Reporting only the result for the threshold

$$\frac{\lambda}{\mu} > \frac{2}{m\langle a\rangle(\psi_w+\gamma_p)+m\sqrt{\langle a\rangle^2(\psi_w-\gamma_p)^2+4\gamma_p\psi_w\langle a^2\rangle}} \tag{3.29}$$

$$R_0 = \frac{\lambda}{\mu}\frac{m\langle a\rangle(\psi_w+\gamma_p)+m\sqrt{\langle a\rangle^2(\psi_w-\gamma_p)^2+4\gamma_p\psi_w\langle a^2\rangle}}{2} > 1 \tag{3.30}$$

In the limiting cases of no one adopting the health intervention, $w = p = 0$, or a zero activity reduction $\psi = \gamma = 1$, the expression of R_0 becomes again equal to the one found in the standard case in (3.23) as expected.
Now, with four new playing variables, becomes interesting to plot phase spaces of R_0. In the case of perfect adoption, everyone is adopting the health intervention, with $p = w = 1$, the variables reduce to two, ψ and γ, and the phase space is shown in figure 3.3. The scale of the two axis is logarithmic and the other variables are chosen in order to represent a disease with $R_0 \approx 3$ when no health intervention are applied. The variation is highlighted by a scale from white to red, with the with the areas with $R_0 = 1$. The areas colored with a light grey are the one representing combination of health intervention stopping the disease to spread, namely $R_0 < 1$. In case of imperfect adoption the structure of the model suggests to plot the phase space also for the fraction of adopters couple p and s. The two phase space are reported in figure 3.4, notice the different scales between the two plot. In the first is reported also the threshold line for the perfect adoption showing how is it the best possible scenario to avoid the beginning of the outbreak. In the second is analyzed the symmetric case with equal reduction both for infected and susceptible, $\psi = \gamma = 0.1$, with a plot showing a decrease in the R_0 values in the right top direction, the one of the perfect adoption, as expected.

The simulation for validating the threshold have been ran for three different combination of adoption 3.5. The point have been chosen looking at the phase space w vs p, in fact only one of them is far enough inside the "red area" of the phase space to highlight a great diffusion. As said before the two type of plots are replicated, and now makes more sense the decision to use the λ on x-axis, it better shows the effects of different combination of health intervention on the specific disease. In the case of R_0 on x-axis plots it is more difficult to highlight this effect. In the plot for the relative variance, the strong health intervention make the end of the lines not flat because of the proximity to the high variance threshold also for the maximum value $\lambda = 1$.Also the maximum is not always exactly on the

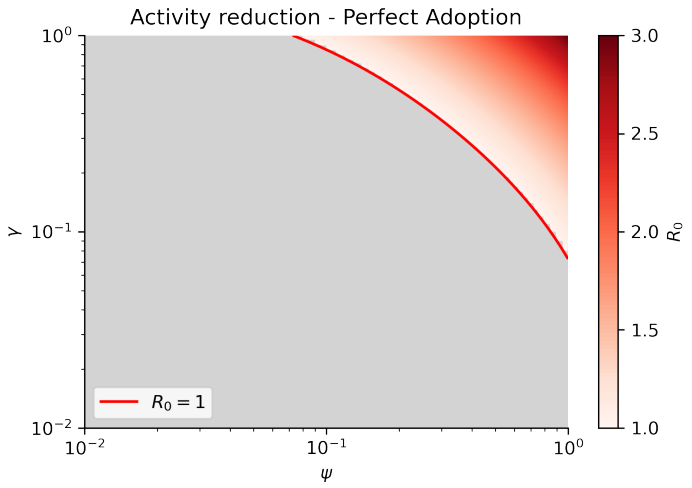

Figure 3.3: Activity reduction perfect random adoption phase space. Plot of the analytical value of the basic reproductive number R_0 obtained in (3.23) in the case of perfect adoption $p = w = 1$, as a function of γ and ψ. Parameters used: $\epsilon = 10^{-3}$, $m = 2$, $\alpha = 2.1$, $\mu = 10^{-2}$ and setting a maximum value of R_0 equal to 3 in case of no adoption.

predicted one, but this is because of the density of points simulated around the predicted threshold.
The chosen values are the same as for the simulation without health intervention with the new two parameters $\psi = 0.1$ and $\gamma = 0.8$.

The other way to distribute the health intervention is to base it on the activity distribution. In particular, if the activity of a vertex is lower to a threshold one the node will reduce her activity. The two threshold can be different based on the compartment type as before, and the reduction too as in the previous case. The two threshold have to be number between 0 and 1, but this time not really comfortable. Indicating with u_s and u_i the threshold for the susceptible and infected compartment respectively, their relation with the fraction of adopters is

$$w = \int H(u_s - a)F(a)\,da = \int_\epsilon^{u_s} F(a)\,da \tag{3.31}$$

$$p = \int H(u_i - a)F(a)\,da = \int_\epsilon^{u_i} F(a)\,da \tag{3.32}$$

with $H(x)$ being the Heaviside function, equal to one when its argument is greater than zero and zero when is lower.

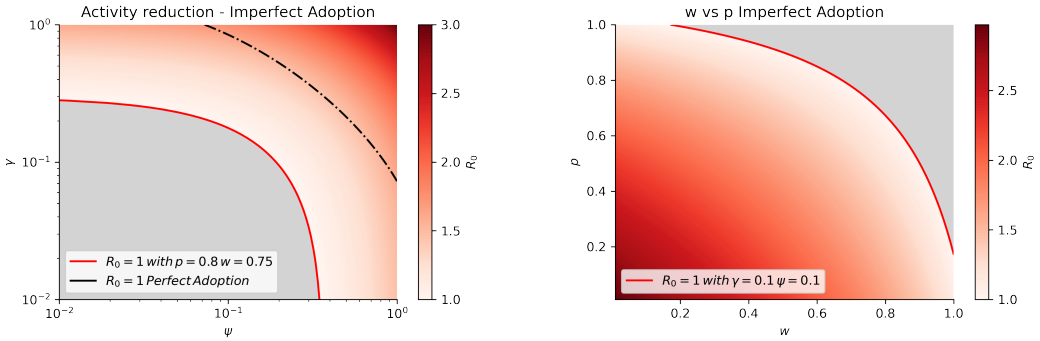

(a) Activity Reduction phase space: γ vs ψ imperfect adoption

(b) Activity Reduction phase space: w vs p imperfect adoption

Figure 3.4: Activity reduction imperfect random adoption phase spaces. Plot of the analytical value of the basic reproductive number R_0 obtained in equation (3.23) in different scenarios. In panel a) R_0 as a function of γ and ψ with $p = 0.8$ and $w = 0.75$. In panel b) R_0 as a function of p and w with $\psi = \gamma = 0.1$. Parameters used in both figures: $\epsilon = 10^{-3}$, $m = 2$, $\alpha = 2.1$, $\mu = 10^{-2}$ and setting a maximum value of R_0 equal to 3 in case of no adoption. A solid red line indicates the threshold $R_0 = 1$, and the dashed black line the threshold in case of prefect adoption.

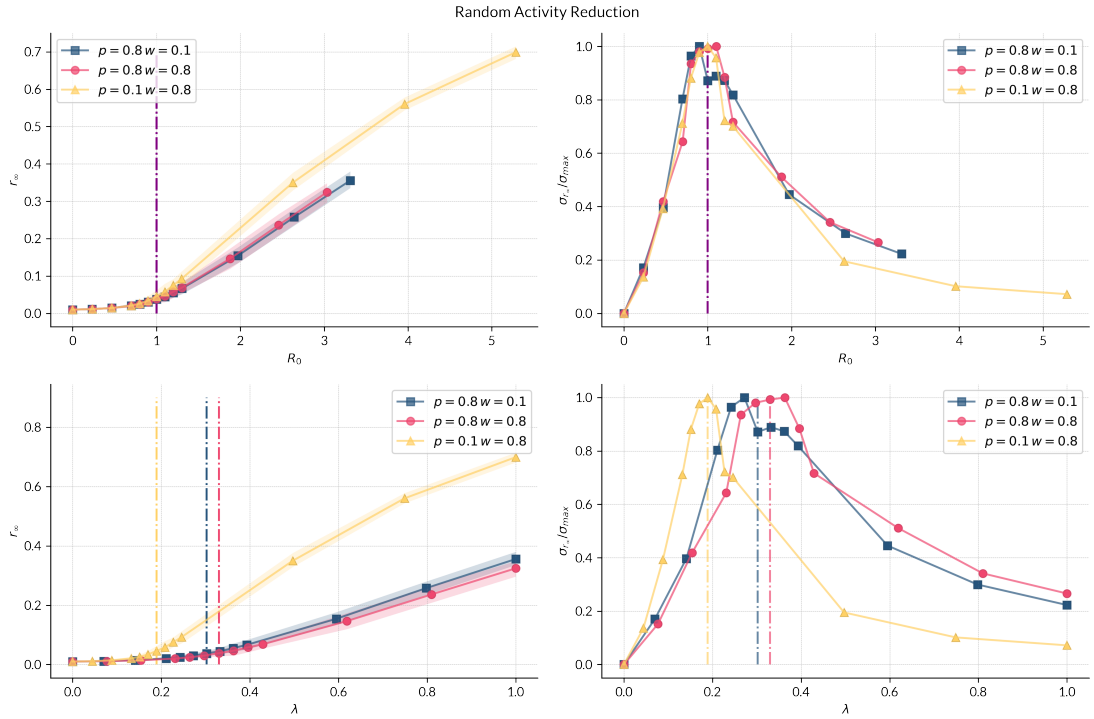

Figure 3.5: Activity reduction random adoption phase transition plot. The plots display on the left the final epidemic size ($r_\infty = R_\infty/N$) with 95% confidence intervals for different values of λ or R_0 in case of non-perfect adoption for different values of p and w. Values of λ are plotted above with the corresponding R_0 values below. Vertical dashed line indicates the analytical threshold derived from (3.29). The plots on the right display the normalized relative variance $\sigma_{r_\infty}/\sigma_{r_\infty}^{max}$ above as a function of λ and below as a function of R_0. Results are obtained by 10^2 stochastic simulation for each point and with the following model parameters: $\mu = 10^{-2}$, $N = 10^5$, $m = 2$, $i_0 = I_0/N = 0.01$ (initial fraction of infected seeds), $\psi = 0.8$ and $\gamma = 0.1$, while for the power law distribution the minimum value $\epsilon = 10^{-3}$, maximum equal to 1, and characteristic power $\alpha = 2.1$

The equation for the evolution of the infected compartment modify in this way

$$\begin{aligned} I_a^{t+\Delta t} &= I_a^t - \mu \Delta t I_a^t + \lambda m \Delta t a \left[1 + (\psi - 1) H(u_s - a)\right] S_a^t \int da \frac{I_a^t}{N} + \\ &+ \lambda m \Delta t S_a^t \int da \left[1 + (\gamma - 1) H(u_i - a)\right] \frac{a I_a^t}{N} \\ I_a^{t+\Delta t} &= I_a^t - \mu \Delta t I_a^t + \lambda m \Delta t a \left[1 + (\psi - 1) H(u_s - a)\right] N_a^t \int da \frac{I_a^t}{N} + \\ &+ \lambda m \Delta t N_a^t \int da \left[1 + (\gamma - 1) H(u_i - a)\right] \frac{a I_a^t}{N} \end{aligned} \tag{3.33}$$

where the expression inside the square brackets is equal to the reduction or to 1 when the the threshold of activity is crossed or not, and the $S_a^t \approx N_a$ approximation have been applied between the lines. The procedure to evaluate the threshold is the same as before with the only difference that in this case the expression of the auxiliary variable Θ has a dependence on the Heaviside function

$$\Theta^t = \int da\ [1 + (\gamma - 1)H(u_i - a)]\ \frac{aI_a^t}{N} \tag{3.34}$$

because of this the second integral have to be taken on $\int da\, a\,[1 + (\gamma - 1)H(n - a)]$ in order to build the equation for Θ.
The total calculation is shown in the appendix B. The threshold in this case reads

$$\frac{\lambda}{\mu} > \frac{2/m}{2 + (\psi - 1)\left\langle a\right\rangle_{\epsilon,u_s} - (\gamma - 1)\left\langle a\right\rangle_{\epsilon,u_i} + \lambda m\sqrt{\mathcal{F}(u_s, \psi, u_i, \gamma)}} \tag{3.35}$$

$$R_0 = \frac{\lambda m}{\mu}\frac{2 + (\psi - 1)\left\langle a\right\rangle_{\epsilon,u_s} - (\gamma - 1)\left\langle a\right\rangle_{\epsilon,u_i} + \lambda m\sqrt{\mathcal{F}(u_s, \psi, u_i, \gamma)}}{2} > 1 \tag{3.36}$$

where the function inside the square root has the form

$$\begin{aligned}\mathcal{F}(u_s, \psi, u_i, \gamma) =&[(1 - \psi)\left\langle a\right\rangle_{\epsilon,u_s} - (1 - \gamma)\left\langle a\right\rangle_{\epsilon,u_i}]^2 - \\ &+4[(\psi - 1)\gamma\left\langle a^2\right\rangle_{\epsilon,u_s} + (\gamma - 1)\left\langle a^2\right\rangle_{\epsilon,u_i} + 1]\end{aligned} \tag{3.37}$$

and the script $\left\langle x\right\rangle_{\epsilon,u}$ indicates the expected value up to u, namely

$$\left\langle x\right\rangle_{\epsilon,u} = \int_\epsilon^u da\, xF(a) \tag{3.38}$$

Observing that $\left\langle x\right\rangle_{\epsilon,1} = \left\langle x\right\rangle$, it is possible to recover the perfect adoption threshold. The phase space plot in 3.6 shows the fundamental role of the more active nodes selected from the tail of the distribution in the spreading of the disease. Only if the top right part of the phase space is zoomed is possible to appreciate a crossing of the threshold Also the threshold simulations highlight this difficulty to stop the spreading, in fact all three the combination of parameters give about the same phase transition in figure 3.7 In this section have been introduced the main methods for the validation of the thresholds in the time-varying activity driven social network framework. In the next chapter will be studied the health intervention introduced in the previous chapter.

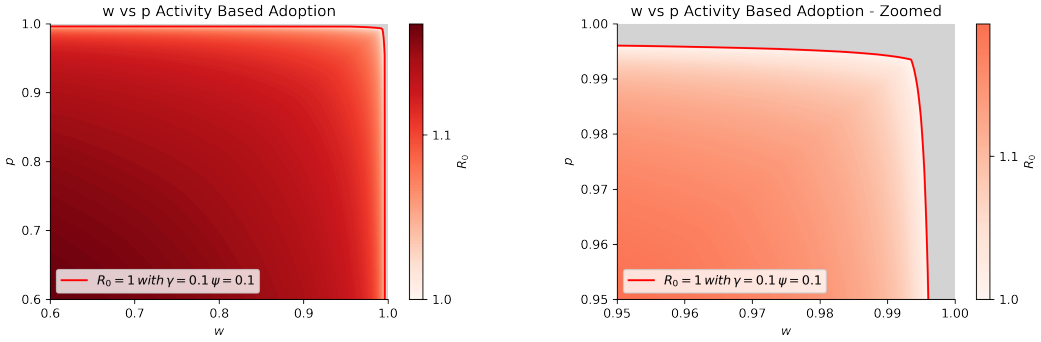

Figure 3.6: Activity reduction imperfect adoption based on nodes' activity phase space. Analytical value of the basic reproductive number R_0 as a function of p and w as obtained in (3.35) in the case of adoption dependent of the nodes' activity, with $\gamma = \psi = 0.1$. The plot on the right highlights a small region of the phase space on the left. Parameters used in both figures: $\epsilon = 10^{-3}$, $m = 2$, $\alpha = 2.1$, $\mu = 10^{-2}$ and setting a maximum value of R_0 equal to 1.2 in case of no adoption. A solid red line indicates the threshold $R_0 = 1$.

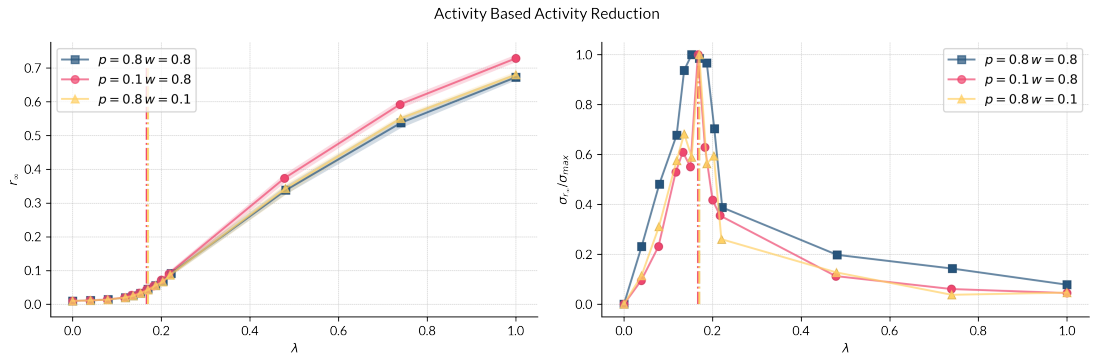

Figure 3.7: Activity reduction with adoption based on nodes' Activity plot. The plots display on the left the final epidemic size ($r_\infty = R_\infty/N$) with 95% confidence intervals for different values of λ in case of non-perfect adoption dependent of nodes' activity for different values of p and w. Vertical dashed line indicates the analytical threshold derived from (3.35). The plots on the right display the normalized relative variance $\sigma_{r_\infty}/\sigma^{max}_{r_\infty}$ as a function of λ. As in the case of non-perfect random adoption in 3.5, results are obtained by 10^2 stochastic simulation for each point and with the following model parameters: $\mu = 10^{-2}$, $N = 10^5$, $m = 2$, $i_0 = I_0/N = 0.01$ (initial fraction of infected seeds), $\psi = 0.8$ and $\gamma = 0.1$, while for the power law distribution the minimum value $\epsilon = 10^{-3}$, maximum equal to 1, and characteristic power $\alpha = 2.1$

Chapter 4

Modeling Health Interventions on Activity Driven Network

4.1 Model the use of face masks in activity driven time-varying social network

4.1.1 Random adoption of face masks case

After we have introduced the approach to model epidemics and evaluate the epidemic threshold in activity driven time-varying networks, we start to model the second health intervention presented in the second chapter: the use of face masks. Face mask are categorized as non pharmaceutical intervention (NPI), and in this thesis we take the assumption of a respiratory virus as SARS-CoV-2. In this section we will study the random adoption case and then the activity based adoption one. In (3.25) have been shown how the use of face mask can affect the transmission rate λ. Now in the activity driven framework, we start with the random adoption considering same parameters:

- α_m is the reduction caused by the face mask, namely 1 minus the effectiveness of the face mask in reducing transmission;
- r_s is the fraction of susceptible using face mask;
- r_i is the fraction of infected using face mask;

Starting from this, the equation for the time evolution of the infected becomes:

$$\begin{aligned} I_a^{t+\Delta t} = I_a^t - \mu\Delta t I_a^t + r_s\alpha\lambda m\Delta t a S_a^t \int da \frac{I_a^t}{N} r_i\alpha_m + r_s\alpha\lambda m\Delta t S_a^t \int da \frac{aI_a^t}{N} r_i\alpha_m + \\ +(1-r_s)\lambda m\Delta t a S_a^t \int da \frac{I_a^t}{N} r_i\alpha_m + (1-r_s)\lambda m\Delta t S_a^t \int da \frac{aI_a^t}{N} r_i\alpha_m + \\ +r_s\alpha_m\lambda m\Delta t a S_a^t \int da \frac{I_a^t}{N}(1-r_i) + r_s\alpha_m\lambda m\Delta t S_a^t \int da \frac{aI_a^t}{N}(1-r_i) + \\ +(1-r_s)\lambda m\Delta t a S_a^t \int da \frac{I_a^t}{N}(1-r_i) + (1-r_s)\lambda m\Delta t S_a^t \int da \frac{aI_a^t}{N}(1-r_i) \end{aligned} \tag{4.1}$$

In the right hand side pf (4.1), after the usual terms $\mu\Delta t I_a^t$, we imagine that the face mask can both reduce susceptibility of S and infectiousness of I, therefore this assumption gives us four different combination terms. In particular the first row represent S and I both wearing mask, the second row S not wearing and I wearing, third row S wearing and I not, last both not wearing. In all the lines the there are two terms, the first term representing when S activates and I receives the link, and the second term vice versa.

$$\begin{aligned} I_a^{t+\Delta t} = I_a^t - \mu\Delta t I_a^t + (r_s\alpha_m + 1 - r_s)\lambda m\Delta t a S_a^t \int da \frac{I_a^t}{N} r_i\alpha_m + \\ +(r_s\alpha_m + 1 - r_s)\lambda m\Delta t S_a^t \int da \frac{aI_a^t}{N} r_i\alpha_m + \\ +(r_s\alpha_m + 1 - r_s)\lambda m\Delta t a S_a^t \int da \frac{I_a^t}{N}(1-r_i) + \\ +(r_s\alpha_m + 1 - r_s)\lambda m\Delta t S_a^t \int da \frac{aI_a^t}{N}(1-r_i) \end{aligned} \tag{4.2}$$

Again we apply the early stage assumption when $S_a^t \sim N_a^t$

$$I_a^{t+\Delta t} = I_a^t - \mu\Delta t I_a^t + \alpha_s\alpha_i\lambda m\Delta t a N_a^t \int da \frac{I_a^t}{N} + \alpha_s\alpha_i\lambda m\Delta t N_a^t \int da \frac{aI_a^t}{N} \tag{4.3}$$

$$with \;\; \alpha_s = 1 - r_s(1-\alpha) \;\; and \;\; \alpha_i = 1 - r_i(1-\alpha)$$

After collecting similar factors, the problem reduce to the one shown in the previous chapter with a multiplicative factor $\alpha_s\alpha_i$ applied to the transmission rate. Therefore, the solution can be directly taken from the standard problem without

health intervention remembering to multiply by $\alpha_s\alpha_i$ the terms presenting λ:

$$\frac{\lambda}{\mu} = \frac{1}{\alpha_s\alpha_i m\left(\langle a\rangle + \sqrt{\langle a^2\rangle}\right)} \tag{4.4}$$

$$R_0 = \frac{\lambda}{\mu} m\alpha_s\alpha_i\left(\langle a\rangle + \sqrt{\langle a^2\rangle}\right) > 1 \tag{4.5}$$

The expressions for α_s and α_i become equal to 1 in case no one is adopting the health intervention, which reduces the expression for R_0 to the one without face masks presented in (2.6). It is interesting to notice the symmetry of R_0 with respect to the fraction of susceptible r_s and infectious r_i adopting face masks. This is possible because the factor α_m (i.e., the effectiveness of the face mask) is the same independently if the individual is a susceptible or an infected. Said differently, we are assuming that the face masks equally reduces susceptibility and infectiousness. In the case of equal fraction of adopters, $r_s = r_i = r \to \alpha_s = \alpha_i = \alpha_r = 1-r(1-\alpha_m)$, the expression for R_0 presents a square in α_r

$$\frac{\lambda}{\mu} = \frac{1}{\alpha_r^2 m\left(\langle a\rangle + \sqrt{\langle a^2\rangle}\right)} \tag{4.6}$$

$$R_0 = \frac{\lambda}{\mu} m\alpha_r^2\left(\langle a\rangle + \sqrt{\langle a^2\rangle}\right) > 1 \tag{4.7}$$

To explore the space of effectiveness of face masks in reducing epidemic spread, we plot the phase space of R_0 as function of r_s and r_i for three different values of effectiveness in 4.1. These values are 10% for the first row plot, 30% in second row, and 50% in the third row. The phase spaces on the left have a combination of parameters with an $R_0 = 3$ without health intervention $r_s = r_i = 0$, and on the right a maximum $R_0 = 1.2$. The $R_0 = 3$ is the same combination used in the phase space activity reduction with random adoption and have been chosen to evidence that the use of face mask only is not sufficient to cross the threshold also with perfect adoption, in case of low values of effectiveness of the face mask. Then on the right we chose to plot the phase space with $R_0 = 1.2$ representing a less transmissible disease, in order to make evident the shape of the transition boundary.
We choose also to run simulation for the evaluation of the phase transition for the three values of effectiveness 4.2. The other parameters are the same of the previous cases, including the fraction of adopters.The plots show the r_∞ mean value and

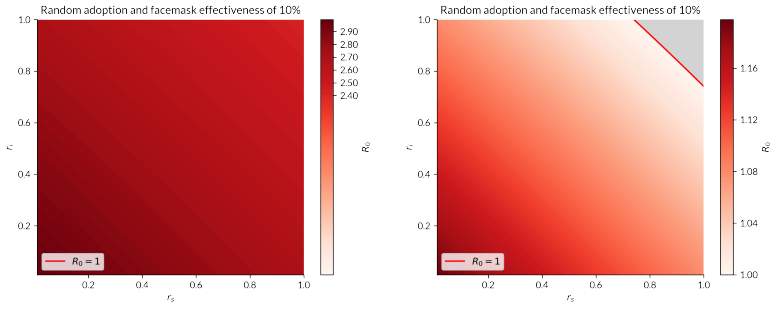

(a)

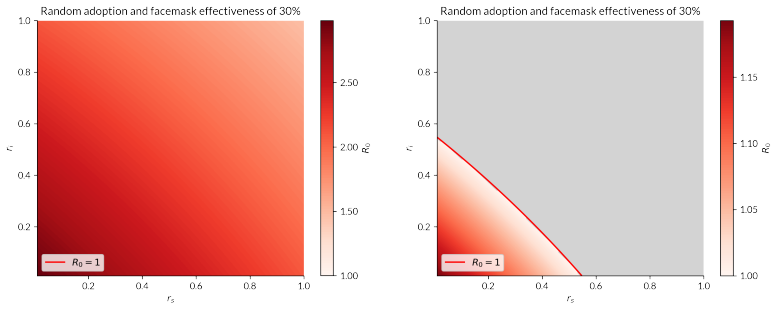

(b)

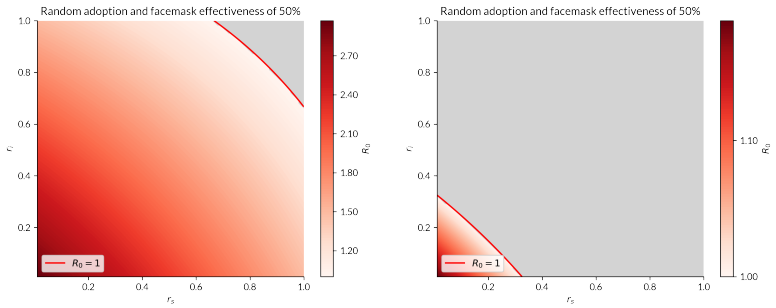

(c)

Figure 4.1: Face mask random adoption phase space. Analytical value of the basic reproductive number R_0 as a function of susceptible adoption fraction r_s and infected adoption fraction r_i as obtained in (4.7) in the case of random adoption, with a) $\alpha_m = 0.9$, b) $\alpha_m = 0.7$, c) $\alpha_m = 0.5$. Parameters used in both figures: $\epsilon = 10^{-3}$, $m = 2$, $\alpha = 2.1$, $\mu = 10^{-2}$ and setting a maximum value of R_0 equal to 3 in case of no adoption on the left, and 1.2 in case of no adoption on the right. A solid red line indicates the threshold $R_0 = 1$.

its relative variance in function of the λ. In the plots is possible to appreciate the symmetry of the problem, in fact it is not possible to distinguish the two lines in which r_s and r_i values are swapped in the r_∞ plot. It is also interesting to see how

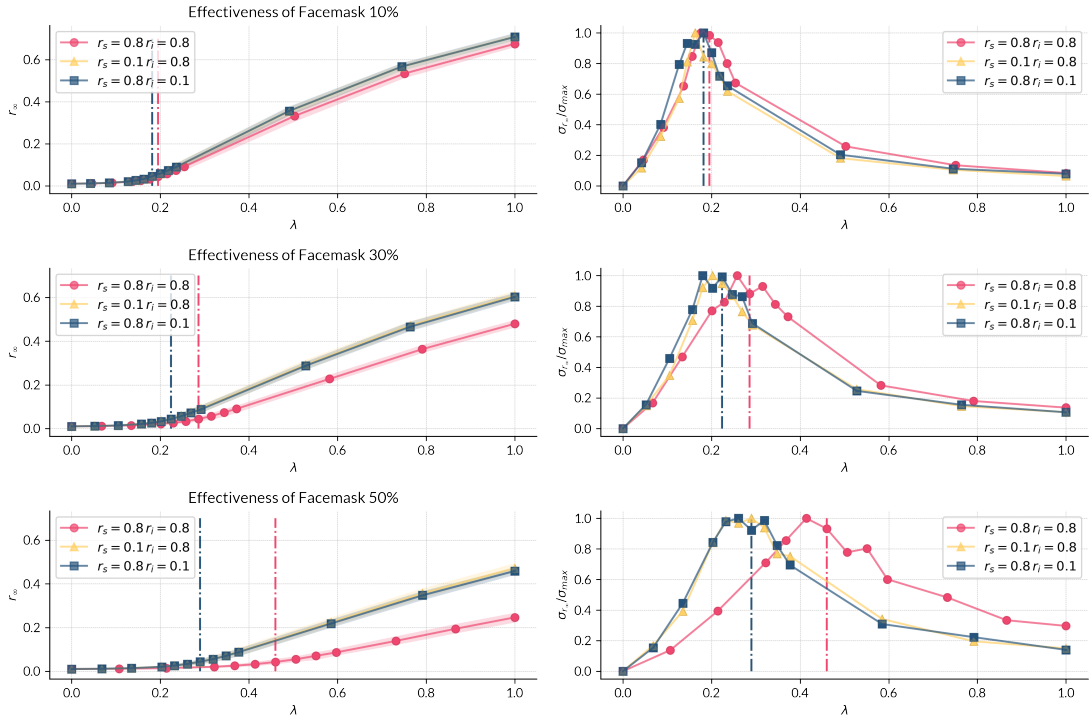

Figure 4.2: Phase transition plot for different values of effectiveness in random adoption face mask. The plots display on the left the final epidemic size ($r_\infty = R_\infty/N$) with 95% confidence intervals for different values of λ in case of non-perfect random adoption different values of r_s and r_i. Vertical dashed line indicates the analytical threshold derived from (4.7). The plots on the right display the normalized relative variance $\sigma_{r_\infty}/\sigma^{max}_{r_\infty}$ as a function of λ. The plots on the first line refer to the case of 10% of effectiveness ($\alpha_m = 0.9$), 30% ($\alpha_m = 0.7$) for the second line, 50% ($\alpha_m = 0.5$) for the third line. Results are obtained by 10^2 stochastic simulation for each point and with the following model parameters: $\mu = 10^{-2}$, $N = 10^5$, $m = 2$, $i_0 = I_0/N = 0.01$ (initial fraction of infected seeds), while for the power law distribution the minimum value $\epsilon = 10^{-3}$, maximum equal to 1, and characteristic power $\alpha = 2.1$

the threshold value λ_t, the one crossing the threshold, depends on the fraction of infected adopting the health intervention, keeping all other parameters fixed. We plotted for four different combination of effectiveness of face mask and adoption fraction in 4.3. These are the combination of α_m equal to 0.5 or 0.9 (effectiveness

of 50% and 10%) and susceptible adoptions r_s of 80% and 10%. The lines look like

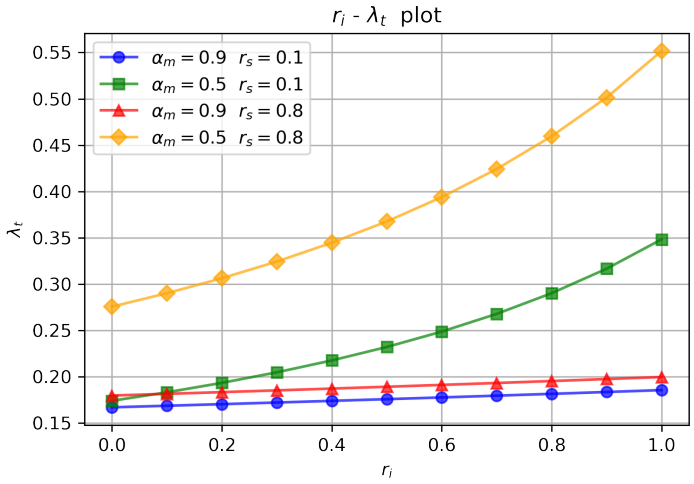

Figure 4.3: Variation of the threshold value λ_t with respect to infect adoption r_i

hyperbolic functions as expected looking at (4.4).

In the next section we replicate the adoption based on node activity in the case of face mask.

4.1.2 Adoption based on activity of face masks

We study here the adoption based on activity, in the case of face mask. We decided to solve analytically the problem in both case of upper limit and lower limit threshold. Indeed, it can be a possible scenario that only more active population, to mitigate their inability to reduce activity, decide to wear face mask. Although that is the most probable case, we wanted to do a general analytical discussion and therefore we also considered the case in which the activity threshold is an upper limit and only those below the threshold wear the mask
Starting from the case in which only nodes lower than a certain activity adopts the health intervention, the general case sees two different thresholds: u_s for susceptible and u_i for infected. The other parameters remain the same as the random adoption case.

The starting equation for this problem is

$$\begin{aligned} I_a^{t+\Delta t} &= I_a^t - \mu \Delta t I_a^t + \\ &+\lambda m \Delta t a [1 + (\alpha_m - 1)H(u_s - a)] S_a^t \int da [1 + (\alpha_m - 1)H(u_i - a)] \frac{I_a^t}{N} + \\ &+\lambda m \Delta t [1 + (\alpha_m - 1)H(u_s - a)] S_a^t \int da [1 + (\alpha_m - 1)H(u_i - a)] \frac{a I_a^t}{N} \end{aligned} \tag{4.8}$$

We are interested in the evaluation of the epidemic threshold so we assume to be at the early stage $S_a^t \sim N_a^t$

$$\begin{aligned} I_a^{t+\Delta t} &= I_a^t - \mu \Delta t I_a^t + \\ &+\lambda m \Delta t a [1 + (\alpha_m - 1)H(u_s - a)] N_a^t \int da [1 + (\alpha_m - 1)H(u_i - a)] \frac{I_a^t}{N} + \\ &+\lambda m \Delta t [1 + (\alpha_m - 1)H(u_s - a)] N_a^t \int da [1 + (\alpha_m - 1)H(u_i - a)] \frac{a I_a^t}{N} \end{aligned} \tag{4.9}$$

where $H(x)$ represent the Heaviside function. In (4.8) the first row of the right hand side is the usual recovering process, the second represents the process of a susceptible activating and establishing a connection with an infected, and the third row represents the infected nodes activating and establishing a connection with a susceptible of activity a.
The next step is the integration over the activity, but differently from the previous cases we integrated over $\int da\,[1 + (\alpha - 1)H(u_i - a)]$, with multiplication by the term containing Heaviside function necessary to have an ODE:

$$\begin{aligned} &\int da [1 + (\alpha_m - 1)H(u_i - a)] I_a^{t+\Delta t} = I_u^{t+\Delta t} = \\ &= \int da\,[1 + (\alpha_m - 1)H(u_i - a)] I_a^t - \mu \Delta t \int da\,[1 + (\alpha_m - 1)H(u_i - a)] I_a^t + \\ &+ \lambda m \Delta t \int da\, a [1 + (\alpha_m - 1)H(u_i - a)][1 + (\alpha - 1)H(u_s - a)] N_a \times \\ &\times \int da'\,[1 + (\alpha_m - 1)H(u_i - a')] \frac{I_{a'}^t}{N} + \\ &+ \lambda m \Delta t \int da\,[1 + (\alpha_m - 1)H(u_i - a)][1 + (\alpha - 1)H(u_s - a)] N_a \times \\ &\times \int da'\,[1 + (\alpha_m - 1)H(u_i - a')] \frac{a' I_{a'}^t}{N} \end{aligned} \tag{4.10}$$

developing the products, we obtained

$$
\begin{aligned}
&I^{t+\Delta t} + (\alpha - 1)\int_{\epsilon}^{u_i} da\, I_a^{t+\Delta t} = I_u^{t+\Delta t} = I_u^t - \mu\Delta t I_u^t + \\
&+ \lambda m \Delta t \int da\, a\, [\, 1 + (\alpha_m - 1)H(u_i - a) + (\alpha_m - 1)H(u_s - a)\,]\, n_a^t I_u^t + \\
&+ \lambda m \Delta t \int da\, a \left[\, (\alpha_m - 1)^2 H(u_i - a)H(u_s - a)\, \right] n_a^t I_u^t + \\
&+ \lambda m \Delta t \int da\, [\, 1 + (\alpha_m - 1)H(u_i - a) + (\alpha_m - 1)H(u_s - a)\,]\, n_a^t \Theta_u^t + \\
&+ \lambda m \Delta t \int da\, \left[\, (\alpha_m - 1)^2 H(u_i - a)H(u_s - a)\, \right] n_a^t \Theta_u^t
\end{aligned}
\tag{4.11}
$$

where $n_a = \frac{N_a}{N}$ is the population fraction and the expression for Θ_u^t is

$$
\Theta_u^t = \int da' [1 + (\alpha - 1)H(u_i - a')] \frac{a' I_{a'}^t}{N} \tag{4.12}
$$

In (4.9) the product of the two Heaviside function can be rewritten as

$$
H(u_i - a)H(u_s - a) = H\left(min\{u_s, u_i\} - a\right) \tag{4.13}
$$

The Heaviside functions can be now deleted changing the extremes of integration, so the equation now becomes

$$
\begin{aligned}
I_u^{t+\Delta t} &= I_u^t - \mu\Delta t I_u^t + \\
&+ \lambda m \Delta t \left\{ \langle a \rangle + (\alpha_m - 1) \left[\int_{\epsilon}^{u_i} da\, a n_a^t + \int_{\epsilon}^{u_s} da\, a n_a^t \right] \right\} I_u^t + \\
&+ \lambda m \Delta t (\alpha_m - 1)^2 \int_{\epsilon}^{min\{u_i, u_s\}} da\, a n_a^t I_u^t + \\
&+ \lambda m \Delta t \left\{ \langle a \rangle + (\alpha_m - 1) \left[\int_{\epsilon}^{u_i} da\, n_a^t + \int_{\epsilon}^{u_s} da\, n_a^t \right] \right\} \Theta_u^t + \\
&+ \lambda m \Delta t + (\alpha_m - 1)^2 \int_{\epsilon}^{min\{u_i, u_s\}} da\, n_a^t \Theta_u^t
\end{aligned}
\tag{4.14}
$$

$$
\begin{aligned}
I_u^{t+\Delta t} &= I_u^t - \mu\Delta t I_u^t + \\
&+ \lambda m \Delta t [\langle a \rangle + (\alpha - 1)(\langle a \rangle_{u_s} + \langle a \rangle_{u_i}) + (\alpha - 1)^2 \langle a \rangle_{min\{u_s, u_i\}}] I_u^t + \\
&+ \lambda m \Delta t [1 + (\alpha - 1)(1_{u_i} + 1_{u_s}) + (\alpha - 1)^2 1_{min\{u_s, u_i\}}] \Theta_u^t
\end{aligned}
\tag{4.15}
$$

$$
I_u^{t+\Delta t} = I_u^t - \mu\Delta t I_u^t + \lambda m \Delta t B(a) I_u^t + \lambda m \Delta t B(1) \Theta_u^t \tag{4.16}
$$

$$\partial_t I_u^t = \mu \Delta t I_u^t + \lambda m \Delta t B(a) I_u^t + \lambda m \Delta t B(1) \Theta_u^t \tag{4.17}$$

where in (4.17) we take the continuous limit and we introduce $B(x)$ function. In $B(x)$ we substituted the thresholds u_s and u_i with u_1 and u_2, being u_1 the minor of the two threshold. This is possible because the two threshold can be swapped without changing the equation. The expression of $B(x)$ reads

$$\begin{aligned} B(x) =& \int da\, x n_a^t + (\alpha_m - 1) \int_\epsilon^{u_2} da\, x n_a^t + \alpha_m(\alpha_m - 1) \int_\epsilon^{u_1} da\, x n_a^t \\ =& \langle x \rangle + (\alpha_m - 1) \langle x \rangle_{u_2} + \alpha_m(\alpha_m - 1) \langle x \rangle_{u_1} \end{aligned} \tag{4.18}$$

example

$$\begin{aligned} B(1) =& \int da\, 1 n_a^t + (\alpha_m - 1) \int_\epsilon^{u_2} da\, 1 n_a^t + \alpha_m(\alpha_m - 1) \int_\epsilon^{u_1} da\, 1 n_a^t \\ =& 1 + (\alpha_m - 1) 1_{u_2} + \alpha_m(\alpha_m - 1) 1_{u_1} \end{aligned} \tag{4.19}$$

and

$$\begin{aligned} B(a) =& \int da\, a n_a^t + (\alpha_m - 1) \int_\epsilon^{u_2} da\, a n_a^t + \alpha_m(\alpha_m - 1) \int_\epsilon^{u_1} da\, a n_a^t \\ =& \langle a \rangle + (\alpha_m - 1) \langle a \rangle_{u_2} + \alpha_m(\alpha_m - 1) \langle a \rangle_{u_1} \end{aligned} \tag{4.20}$$

in these expressions the subscript indicates that the integral is evaluated from ϵ up to the subscript (e.g., when the argument is 1 it indicates the total population below the subscript).
Notice that the dynamic equation, differently from the cases studied up to now, is not for the whole population of infected compartment but for a fraction. Considering that the solution of this is a sum of exponentials, the leading exponential remain the one defining the threshold. What is not anymore precise is the predicted steepness of the early stage because of the difference with a fraction of infected described by the equations.

We now integrate (4.9) over $\int da\, a[1 + (\alpha_m - 1)H(u_i - a)]$ in order to have an

equation for Θ_u^t

$$\begin{aligned}
&\int da[1+(\alpha-1)H(u_i-a)]aI_a^{t+\Delta t} = \Theta_u^{t+\Delta t} = \\
&= \int da[1+(\alpha-1)H(u_i-a)]aI_a^t - \mu\Delta t \int da[1+(\alpha-1)H(u_i-a)]aI_a^t + \\
&+ \lambda m\Delta t \int da[1+(\alpha-1)H(u_i-a)][1+(\alpha-1)H(u_s-a)]a^2N_a^t \times \\
&\times \int da'[1+(\alpha-1)H(u_i-a')]\frac{I_{a'}^t}{N} + \\
&+ \lambda m\Delta t \int da[1+(\alpha-1)H(u_s-a)][1+(\alpha-1)H(u_i-a)]aN_a^t \times \\
&\times \int da'[1+(\alpha-1)H(u_i-a')]\frac{a'I_{a'}^t}{N}
\end{aligned} \tag{4.21}$$

Repeating the calculation in a way similar to (4.14) and (4.15), we reach the expression

$$\Theta^{t+\Delta t} = \Theta^t - \mu\Delta t\Theta^t + \lambda m\Delta t B(a^2)I_u^t + \lambda m\Delta t B(a)\Theta_u^t \tag{4.22}$$

which taking the continuous limit becomes

$$\partial_t\Theta_u^t = -\mu\Theta^t + \lambda m B(a^2)I_u^t + \lambda m B(a)\Theta_u^t \tag{4.23}$$

$$\begin{bmatrix}\partial_t I_u^t \\ \partial_t\Theta^t\end{bmatrix} = \begin{bmatrix}-\mu+\lambda mF(a) & \lambda mF(1) \\ \lambda mF(a^2) & -\mu+\lambda mF(a)\end{bmatrix}\begin{bmatrix}I_u^t \\ \Theta^t\end{bmatrix} \tag{4.24}$$

To find the threshold value we have to find the maximum eigenvalue of the matrix, and impose it greater than zero. Remember that to simplify the calculation the transformation $\Lambda' = \frac{\Lambda+\mu}{\lambda m}$ have been applied

$$[B(a)-\Lambda']^2 - B(1)B(a^2) = 0 \tag{4.25}$$

$$\Lambda'^2 - 2B(a)\Lambda' + B(a)^2 - B(1)B(a^2) = 0 \tag{4.26}$$

After transforming back the eigenvalue

$$\Lambda = -\mu + \lambda m[B(a) + \sqrt{B(1)B(a^2)}] \tag{4.27}$$

The threshold expression reads

$$\frac{\lambda}{\mu} > \frac{1}{m[B(a)+\sqrt{B(1)B(a^2)}]} \tag{4.28}$$

$$R_0 = \frac{\lambda m}{\mu}[B(a)+\sqrt{B(1)B(a^2)}] > 1 \tag{4.29}$$

The threshold value expression is symmetric to the swap of fractions of infected and susceptible.
After writing the equation for the problem in case the population adopting the use of face mask is above the threshold in (4.30), we noticed that the pattern in the solution is similar, with the only difference in the auxiliary function that this time we called $\mathfrak{A}(x)$ (4.31), in which the minimum is substituted with the maximum between the two threshold u_i and u_S

$$\begin{aligned} I_a^{t+\Delta t} = & I_a^t - \mu \Delta t I_a^t + \\ & + \lambda m \Delta t a [1 + (\alpha_m - 1) H(a - u_s)] N_a^t \int da\, [1 + (\alpha_m - 1) H(a - u_i)] \frac{I_a^t}{N} + \\ & + \lambda m \Delta t [1 + (\alpha_m - 1) H(a - u_s)] N_a^t \int da [1 + (\alpha_m - 1) H(a - u_i)] \frac{a I_a^t}{N} \end{aligned} \tag{4.30}$$

$$\begin{aligned} \mathfrak{A}(x) = & \int da\, x n_a^t + (\alpha_m - 1) \int_{u_1}^1 da\, x n_a^t + \alpha_m (\alpha_m - 1) \int_{u_2}^1 da\, x n_a^t \\ = & x + (\alpha_m - 1) x_{\overline{u_1}} + \alpha (\alpha_m - 1) x_{\overline{u_2}} \end{aligned} \tag{4.31}$$

example

$$\begin{aligned} \mathfrak{A}(1) = & \int da\, 1 n_a^t + (\alpha_m - 1) \int_{u_1}^1 da\, 1 n_a^t + \alpha_m (\alpha_m - 1) \int_{u_2}^1 da\, 1 n_a^t \\ = & 1 + (\alpha_m - 1) 1_{\overline{u_1}} + \alpha_m (\alpha_m - 1) n_{\overline{u_2}} \end{aligned} \tag{4.32}$$

and

$$\begin{aligned} \mathfrak{A}(a) = & \int da\, a n_a^t + (\alpha_m - 1) \int_{\epsilon}^{u_2} da\, a n_a^t + \alpha_m (\alpha_m - 1) \int_{\epsilon}^{u_1} da\, a n_a^t \\ = & a + (\alpha_m - 1) a_{\overline{u_1}} + \alpha_m (\alpha_m - 1) a_{\overline{u_2}} \end{aligned} \tag{4.33}$$

And the threshold is straightforward similar to the previous case but with this new auxiliary function

$$\frac{\lambda}{\mu} > \frac{1}{m[\mathfrak{A}(a) + \sqrt{\mathfrak{A}(1)\mathfrak{A}(a^2)}]} \tag{4.34}$$

$$R_0 = \frac{\lambda m}{\mu} [\mathfrak{A}(a) + \sqrt{\mathfrak{A}(n)\mathfrak{A}(a^2)}] > 1 \tag{4.35}$$

We plotted the phase space of the epidemic threshold in function of the activity thresholds for susceptibles r_s and infected r_i, both for the two types of adoption. We chose to always use the maximum value $R_0 = 1.75$, and on the left represent the effects of the upper activity threshold and on the right the lower one. In the first row the effectiveness of the mask is 10%, $\alpha_m = 0.9$, and in both cases also

with perfect adoption do not cross the threshold value for the disease. Different the cases for the 30% and 50% of effectiveness, when the threshold is crossed. In these 4 plot is shown also the black dotted line corresponding to the $R_0 = 1$ line in the case of random adoption. The random adoption is always positioned between the two activity based adoption. This because in a case the most active nodes use face mask while in the other they do not use it. We proceed with the validation of the analytical threshold with simulations. We chose to plot the same values as in the activity reduction case 3.5, in particular the case with $r_s = r_i = 0.8$, $r_s = 0.1$ and $r_i = 0.8$, and the symmetric one with $r_s = 0.8$ and $r_i = 0.1$, combined with effectiveness of 10%, 20% and 50%. As expected the phase transition happens in the same point but with a steepness greater in the case of greater adoption of the susceptible in both figures 4.12 and 4.11.

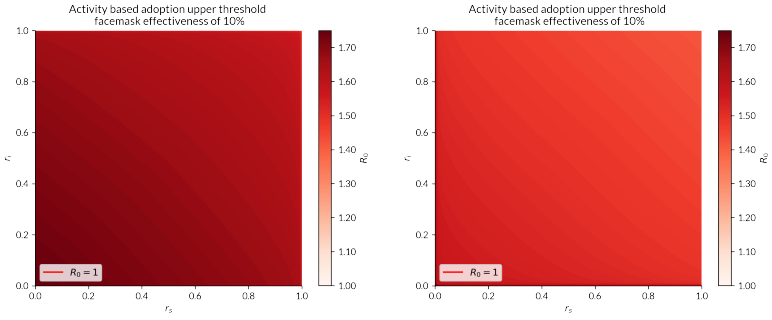

(a)

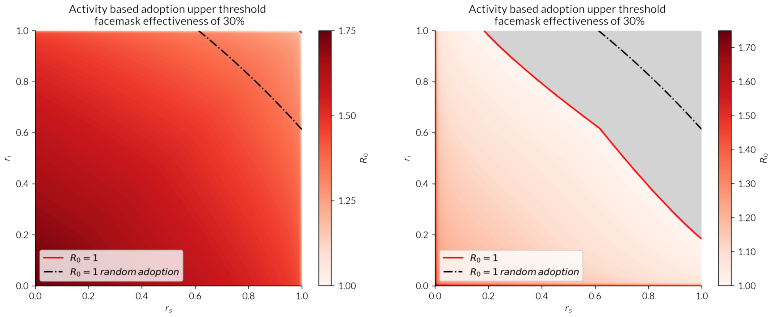

(b)

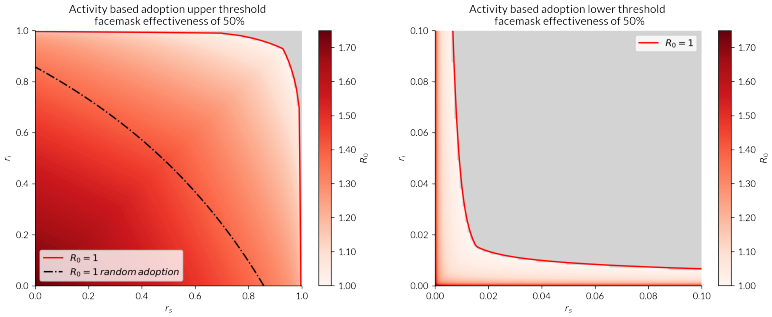

(c)

Figure 4.4: Face mask activity based adoption phase space. Analytical value of the basic reproductive number R_0 in the case of adoption based on activity as a function of susceptible adopters fraction r_s and infected adopters fraction r_i as obtained in (4.29) with upper threshold on the left and (4.35) with lower threshold on the right, with a) $\alpha_m = 0.9$, b)$\alpha_m = 0.7$, c) $\alpha_m = 0.5$. Parameters used in both figures: $\epsilon = 10^{-3}$, $m = 2$, $\alpha = 2.1$, $\mu = 10^{-2}$ and setting a maximum value of R_0 equal to 1.75 in case of no adoption. A solid red line indicates the threshold $R_0 = 1$, and the dashed black line the threshold line for the random adoption case.

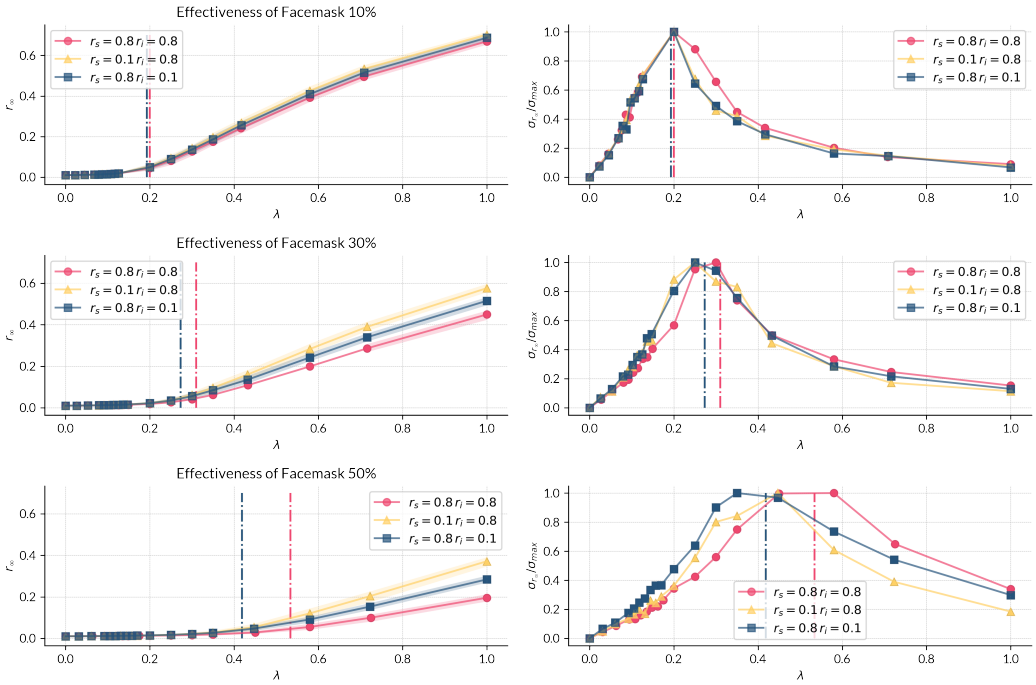

Figure 4.5: Lower threshold activity based adoption phase space for face mask. The plots display on the left the final epidemic size ($r_\infty = R_\infty/N$) with 95% confidence intervals for different values of λ in case of non-perfect adoption dependent on nodes' activity, with adopters **above** a certain activity threshold. The threshold is selected for different values of r_s and r_i. Vertical dashed line indicates the analytical threshold derived from (4.29). The plots on the right display the normalized relative variance $\sigma_{r_\infty}/\sigma^{max}_{r_\infty}$ as a function of λ. The plots on the first line refer to the case of 10% of effectiveness ($\alpha_m = 0.9$), 30% ($\alpha_m = 0.7$) for the second line, 50% ($\alpha_m = 0.5$) for the third line. Results are obtained by 10^2 stochastic simulation for each point and with the following model parameters: $\mu = 10^{-2}$, $N = 10^5$, $m = 2$, $i_0 = I_0/N = 0.01$ (initial fraction of infected seeds), while for the power law distribution the minimum value $\epsilon = 10^{-3}$, maximum equal to 1, and characteristic power $\alpha = 2.1$

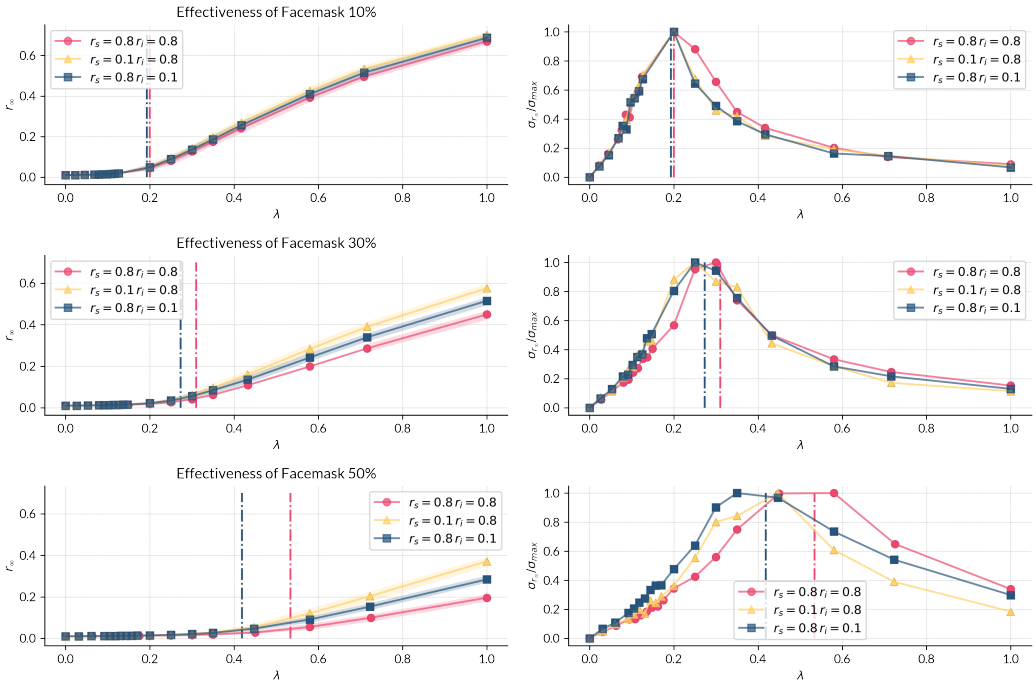

Figure 4.6: Upper threshold activity base adoption phase space for face mask. The plots display on the left the final epidemic size ($r_\infty = R_\infty/N$) with 95% confidence intervals for different values of λ in case of non-perfect adoption dependent on nodes' activity, with adopters **below** a certain activity threshold. The threshold is selected for different values of r_s and r_i. Vertical dashed line indicates the analytical threshold derived from (4.35). The plots on the right display the normalized relative variance $\sigma_{r_\infty}/\sigma^{max}_{r_\infty}$ as a function of λ. The plots on the first line refer to the case of 10% of effectiveness ($\alpha_m = 0.9$), 30% ($\alpha_m = 0.7$) for the second line, 50% ($\alpha_m = 0.5$) for the third line. Results are obtained by 10^2 stochastic simulation for each point and with the following model parameters: $\mu = 10^{-2}$, $N = 10^5$, $m = 2$, $i_0 = I_0/N = 0.01$ (initial fraction of infected seeds), while for the power law distribution the minimum value $\epsilon = 10^{-3}$, maximum equal to 1, and characteristic power $\alpha = 2.1$

4.2 Model vaccination in activity driven time-varying social network

4.2.1 Random adoption of vaccination

We modeled the vaccination campaign as a single shot before the beginning of the simulation.

The parameters of the simulations introduced also in chapter 3 are the fraction of susceptible f joins the vaccine campaign and once vaccinated, each node have a probability v to leave the S compartment and enter in a new compartment R_v and eliminating the possibility to become infected. The properties of individuals in R_v are exactly the same of the individuals in R, we choose to create a new compartment to have the possibility to count the total faction of infected during the stimulation looking directly at R compartment for $t \to \infty$, namely $i_\infty = r_\infty$. Being f a fraction and v a probability, both are number between zero and 1. We first saw their influence in the approximation of S_a^t, in fact the equation for N_t^a now has to take into account the presence of R_v compartment, that is not negligible. Now the approximation of the susceptible reads

$$S_a^t \sim N_a^t - R_{v_a}^t = N_a^t - vfN_a^t = (1 - vf)N_a^t \tag{4.36}$$

The approximations enter in the equation for the dynamics of Infected giving

$$\begin{aligned} I_a^{t+\Delta t} = I_a^t - \mu \Delta t I_a^t + (1 - vf)\lambda m \Delta t a N_a^t \int da \frac{I_a^t}{N} \\ + (1 - vf)\lambda m \Delta t N_a^t \int da \frac{a I_a^t}{N} \end{aligned} \tag{4.37}$$

We see the term $(1 - vf)$ could be incorporated into the m constant being only a multiplicative factor, in this case the equation for the threshold is evaluated straightforward from the one of the case without health intervention in (3.23)

$$\frac{\lambda}{\mu} = \frac{1}{(1 - vf)\left[m(\langle a \rangle + \sqrt{\langle a^2 \rangle}\right]} \tag{4.38}$$

$$R_0 = \frac{\lambda}{\mu} m(1 - vf)\left[\langle a \rangle + \sqrt{\langle a^2 \rangle}\right] > 1 \tag{4.39}$$

The factor $1 - vf$ is always less or equal than zero, confirming is effect of reducing the threshold, and in the limiting cases of no effectiveness $f = 0$ or no vaccination campaign $v = 0$ the threshold gives back the original one.
in figure **??** we plotted the phase space of the above equation. On the axes are reported the values of f and v between zero and 1. As in the case for face mask random adoption we reported the phase space for a disease that without health intervention have $R_0 = 3$ on the left, and $R_0 = 1.2$ on the right. Comparing with them we see that it is always possible to cross the threshold stopping the diffusion also for larger values of R_0, not possible in some cases for the use of face masks.

We ran the simulation for combination of values of 40% and 80% in the adoption and values of 50%, 70% and 90% in the effectiveness. The results reported in the

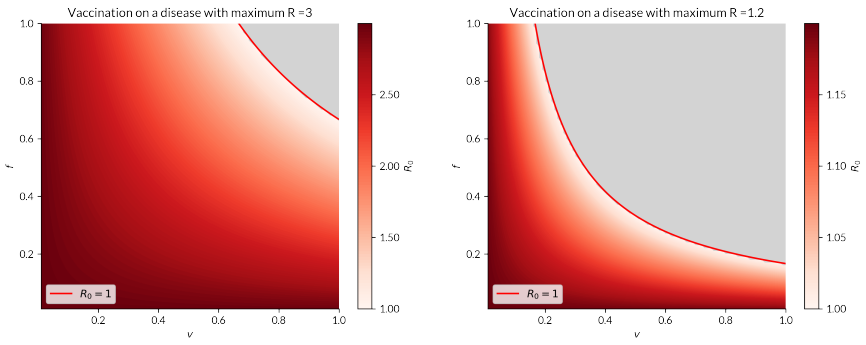

Figure 4.7: Vaccine random adoption phase space. Analytical value of the basic reproductive number R_0 as a function of adoption fraction f and effectiveness v as obtained in (4.39) in the case of random adoption. Parameters used in both figures: $\epsilon = 10^{-3}$, $m = 2$, $\alpha = 2.1$, $\mu = 10^{-2}$ and setting a maximum value of R_0 equal to 3 in case of no adoption on the left, and 1.2 in case of no adoption on the right. A solid red line indicates the threshold $R_0 = 1$.

phase space plots in 4.8 show the phase transition in six different scenarios in the plots on the left. In the plot on the right, the relative variance shows again its maximum at the threshold values predicted. It is interesting to see that in the case with 90% of effectiveness and 80% of adoption, the relative variance plotted line does not flatten as in the other case, this is justified by the fact that also the extreme values of $\lambda = 1$ are still near the threshold values and suffer from the phase transition fluctuations. The values of the thresholds λ_t are plotted with respect to vaccine effectiveness in the figure 4.9. It shows the values near to 1 reached in the case of adoption equal to 80% and as expected has the shape of a reflected branch hyperbola .

4.2.2 Adoption based on activity of vaccination

In this section we try to model an adoption based on activity for the vaccination as done for the previous health intervention. Differently from the case of facemask activity based adoption, in which there were two different equations for the above threshold activation (4.9) and the below threshold activation (4.30), for the vaccination we chose to group them in a single equation.
The model as in the facemask case has only one threshold f, but we introduced two more parameters, $f_>$ and $f_<$, indicating respectively the random fraction of adopters above the threshold activity and the random fraction of adopters below. Both, are of course values between zero and one. The equation for approximating

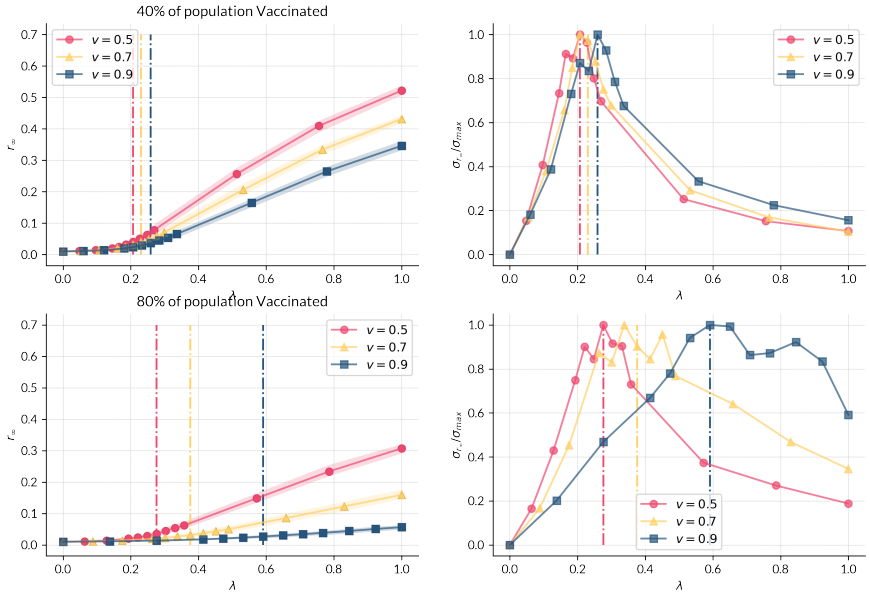

Figure 4.8: Vaccine random adoption phase transition plot. The plots display on the left the final epidemic size ($r_\infty = R_\infty/N$) with 95% confidence intervals for different values of λ in case of non-perfect random adoption and different values of effectiveness f. Vertical dashed line indicates the analytical threshold derived from (4.39). The plots on the right display the normalized relative variance $\sigma_{r_\infty}/\sigma^{max}_{r_\infty}$ as a function of λ. The plots on the first line refer to the case of 40% of adoption, and in the second line of 80% of adoption. Results are obtained by 10^2 stochastic simulation for each point and with the following model parameters: $\mu = 10^{-2}$, $N = 10^5$, $m = 2$, $i_0 = I_0/N = 0.01$ (initial fraction of infected seeds), while for the power law distribution the minimum value $\epsilon = 10^{-3}$, maximum equal to 1, and characteristic power $\alpha = 2.1$

now becomes

$$\begin{aligned} S_a^t \sim N_a^t - R_a^t =& N_a^t - v[f_> + (f_< - f_>)H(u-a)]N_a^t = \\ =& \{1 - v[f_> + (f_< - f_>)H(u-a)]\}N_a^t \end{aligned} \tag{4.40}$$

where $H(x)$ is the Heaviside function introduced for modeling the effect of the threshold. Is straightforward to see that the case of total random adoption is recovered when $f_> = f_<$. While the separated cases presented for face masks activity based adoption are reached in the case of $f_< = 0$ and $f_> = 1$ for the above threshold activation, and in $f_< = 1$, $f_> = 0$ for the below threshold activation.

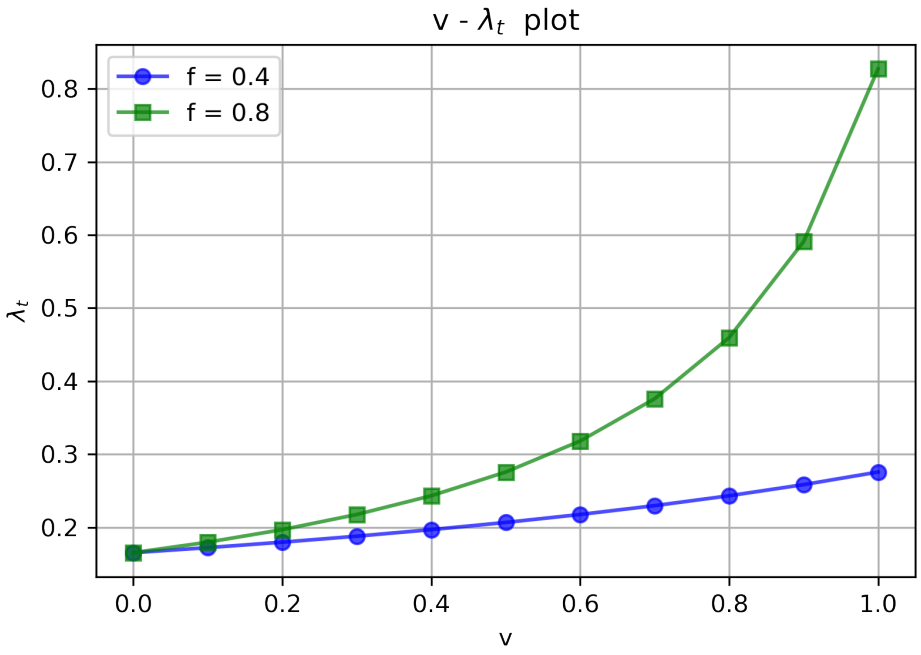

Figure 4.9: Variation of the threshold value λ_t with respect to vaccine effectiveness v

Proceeding with the development of the model, the equation for the dynamics of infected in the general case becomes

$$I_a^{t+\Delta t} = I_a^t - \mu \Delta t I_a^t + \{1 - v[f_> + (f_< - f_>)H(u-a)]\}\lambda m \Delta t a N_a^t \int da \frac{I_a^t}{N} + \\ + \{1 - v[f_> + (f_< - f_>)H(u-a)]\}\lambda m \Delta t N_a^t \int da \frac{a I_a^t}{N} \tag{4.41}$$

The integral terms do not present the Heaviside terms so we proceed integrating in $\int da$ both sides

$$\begin{aligned}\int da I_a^{t+\Delta t} &= \int da\, I_a^t - \mu\Delta t \int da\, I_a^t \\ &+ \lambda m\Delta t \int da\, a\{1 - v[f_> + (f_< - f_>)H(u-a)]\}N_a^t \int da' \frac{I_{a'}^t}{N} + \\ &+ \lambda m\Delta t \int da\, \{1 - v[f_> + (f_< - f_>)H(u-a)]\}N_a^t \int da' \frac{aI_{a'}^t}{N} \end{aligned} \tag{4.42}$$

$$\begin{aligned} I^{t+\Delta t} &= I^t - \mu\Delta t I^t + \\ &+ \lambda m\Delta t \int da\, a(1 - vf_>)n_a^t + \lambda m\Delta t \int_\epsilon^u da\, a(f_> - f_<)n_a^t I^t + \\ &+ \lambda m\Delta t \int da(1 - vf_>)n_a^t \Theta^t + \lambda m\Delta t \int_\epsilon^u dav(f_> - f_<)n_a^t \Theta^t \end{aligned} \tag{4.43}$$

$$\begin{aligned} I^{t+\Delta t} &= I^t - \mu\Delta t I^t + \lambda m\Delta t[(1 - vf_>)\langle a\rangle + v(f_> - f_<)\langle a\rangle_u]I^t + \\ &+ \lambda m\Delta t[(1 - vf_>)1 + v(f_> - f_<)1_u]\Theta^t \end{aligned} \tag{4.44}$$

with

$$\Theta^t = \int da' \frac{a' I_{a'}^t}{N} \tag{4.45}$$

To write the equation for Θ^t, integrate in $\int a\, da$

$$\begin{aligned} &\int da\, aI_a^{t+\Delta t} = \int da\, aI_a^t - \mu\Delta t \int da\, aI_a^t + \\ &+ \lambda m\Delta t \int da\, a^2\{1 - v[f_> + (f_< - f_>)H(u-a)]\}N_a \int da' \frac{I_{a'}^t}{N} + \\ &+ \lambda m\Delta t \int da\{1 - v[f_> + (f_< - f_>)H(u-a)]\}N_a \int da' \frac{aI_{a'}^t}{N} \end{aligned} \tag{4.46}$$

$$\begin{aligned} &\Theta^{t+\Delta t} = \Theta^t - \mu\Delta t\Theta^t + \\ &+ \lambda m\Delta t \int da\, a^2(1 - vf_>)n_a + \lambda m\Delta t \int_\epsilon^u da\, a^2(f_> - f_<)n_a I^t + \\ &+ \lambda m\Delta t \int da\, a(1 - vf_>)n_a\Theta^t + \lambda m\Delta t \int_\epsilon^u da\, av(f_> - f_<)n_a\Theta^t \end{aligned} \tag{4.47}$$

$$\begin{aligned} &\Theta^{t+\Delta t} = \Theta^t - \mu\Delta t\Theta^t + \\ &+ \lambda m\Delta t[(1 - vf_>)\left\langle a^2\right\rangle + v(f_> - f_<)\left\langle a^2\right\rangle_u]I^t + \\ &+ \lambda m\Delta t[(1 - vf_>)\langle a\rangle + v(f_> - f_<)\langle a\rangle_u]\Theta^t \end{aligned} \tag{4.48}$$

Both in the equation for I^t and Θ^t we recognize a pattern in the multiplicative terms that are synthesized in the function $V(x)$

$$\begin{aligned} V(x) &= \int da\, x(1-vf_>)n_a^t + \int_\epsilon^u da\, xv(f_> - f_<)n_a^t = \\ &= (1-vf_>)\langle x\rangle + v(f_> - f_<)\langle x\rangle_u \end{aligned} \tag{4.49}$$

example

$$\begin{aligned} V(1) &= \int da\, 1(1-vf_>)n_a^t + \int_\epsilon^u da\, 1v(f_> - f_<)n_a^t = \\ &= (1-vf_>)1 + v(f_> - f_<)1_u \end{aligned} \tag{4.50}$$

and

$$\begin{aligned} V(a) &= \int da\, a(1-vf_>)n_a^t + \int_\epsilon^u da\, av(f_> - f_<)n_a^t = \\ &= (1-vf_>)\langle a\rangle + v(f_> - f_<)\langle a\rangle_u \end{aligned} \tag{4.51}$$

$$\begin{aligned} V(a^2) &= \int da\, a^2(1-vf_>)n_a^t + \int_\epsilon^u da\, a^2v(f_> - f_<)n_a^t = \\ &= (1-vf_>)\left\langle a^2\right\rangle + v(f_> - f_<)\left\langle a^2\right\rangle_u \end{aligned} \tag{4.52}$$

where the subscript u indicates the average of the variable from the lower limit value of the activity distribution ϵ up to the u upper threshold value.
Recasting and taking the continuous limit, the equations become

$$\partial_t I^t = -\mu I^t + \lambda m V(a) I^t + \lambda m V(1)\Theta^t \tag{4.53}$$

$$\partial_t \Theta^t = -\mu \Theta^t + \lambda m V(a) I^t + \lambda m V(a^2)\Theta^t \tag{4.54}$$

The system written in matrix form reads

$$\begin{bmatrix} \partial_t I^t \\ \partial_t \Theta^t \end{bmatrix} = \begin{bmatrix} -\mu + \lambda m V(a) & \lambda m V(1) \\ \lambda m V(a^2) & -\mu + \lambda m V(a) \end{bmatrix} \begin{bmatrix} I^t \\ \Theta^t \end{bmatrix} \tag{4.55}$$

Again to find the leading exponential term of the solution we need to find the largest eigenvalue Λ of the matrix

$$[V(a) - \Lambda']^2 - V(1)V(a^2) = 0 \tag{4.56}$$

$$\Lambda'^2 - 2V(a)\Lambda' + V(a)^2 - V(1)V(a^2) = 0 \tag{4.57}$$

Where the form with + has already been selected to find the maximum eigenvalue, and $\Lambda' = \frac{\Lambda+\mu}{\lambda m}$. After transforming it we obtain the expression

$$\Lambda = -\mu + \lambda m \left[V(a) + \sqrt{V(1)V(a^2)}\right] \tag{4.58}$$

And the threshold condition reads

$$\frac{\lambda}{\mu} > \frac{1}{m\left[V(a) + \sqrt{V(1)V(a^2)}\right]} \tag{4.59}$$

$$R_0 = \frac{\lambda m}{\mu}\left[V(a) + \sqrt{V(1)V(a^2)}\right] > 1 \tag{4.60}$$

As shown before, turning off the health intervention gives back the expression for the no reduction, in fact $V(x)$ in these cases assumes the value of $\langle x \rangle$. Being a more general case it contain also the expression for the random adoption case when $f_< = f_>$.
With continuity with the examples used up to now, we decide to show the results for the cases of only upper threshold activation and only lower threshold activation. In figure 4.10 the color-maps show a disease with maximum value of $R_0 = 3$ on the left and $R_0 = 1.2$ on the right. The color maps in the first line are for adopters below the threshold activity and in the second line are the in the case of adopters above the threshold activity. The red line in the plots represent the phase transition bound for the model, and the dotted black line represent the one for the corresponding random adoption for vaccines. See how the random adoption always has a better effect in mitigating the disease with respect the below threshold health intervention, while above threshold health activation is preferred to the random case. This is in according with the fact that the more active individuals are the super-spreaders, and their joining to the vaccination campaign is relevant in the lowering of the R_0.

Also for the vaccination we ran simulation in both cases, lower threshold in figure 4.11, and upper threshold in figure 4.12. The combination of the two parameters is the same we tested for the random adoption: adoption of 40% and 80%, and effectiveness of the vaccine of 50%, 70% and 90%. The phase transition in the first case happens for values of λ shifted to the right with respect to the case of the upper threshold, up to the case with 90% of effectiveness and 40% effectiveness (blue line in the upper 4.12) and 70% of effectiveness and 80% of adoption (yellow line in the lower same figure) that remain way into the transition phase looking at relative variance still near to one for high values of λ. In particular the case 80% adoption upper threshold and 90% of effectiveness in blue line even surpasses the $\lambda = 1$ maximum case for the simulation. Considering the values of vaccine in the covid-19 pandemics for vaccine effectiveness to be between the 70% and 90% of effectiveness also at first dose and overcoming the 90% with more doses[30], a vaccination campaign involving a great percentage of the population could mitigate also disease with great values of R_0 protecting in this way the more sensible part of the population.

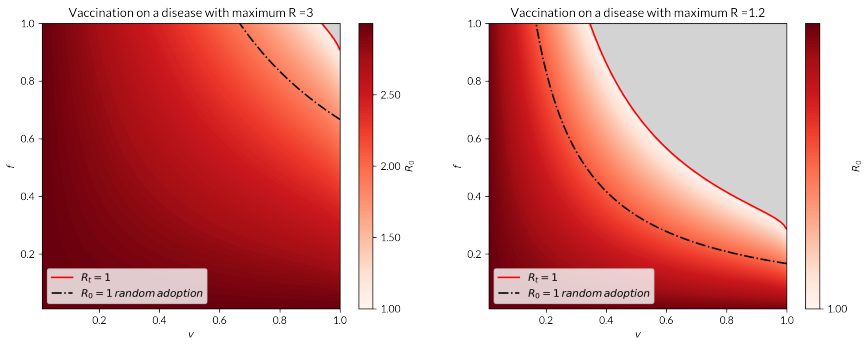

(a) Below threshold activity based adoption

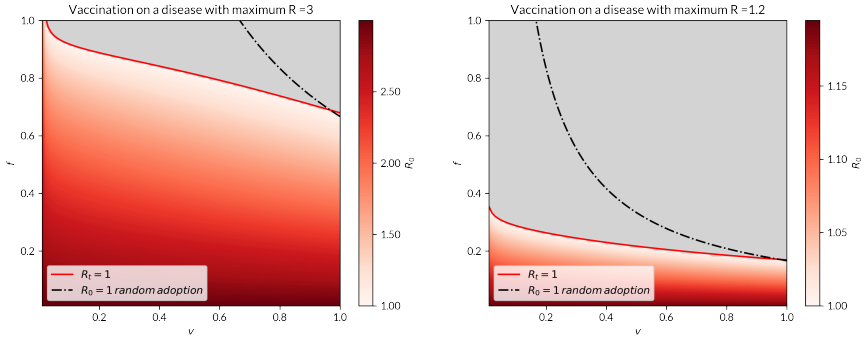

(b) Above threshold activity based adoption

Figure 4.10: Vaccine activity based adoption phase space. Analytical value of the basic reproductive number R_0 in the case of adoption based on activity as a function of adopters fraction f and vaccine effectiveness v as obtained in (4.60) with a) upper threshold for the activity and b) lower threshold for the threshold. Parameters used in both figures: $\epsilon = 10^{-3}$, $m = 2$, $\alpha = 2.1$, $\mu = 10^{-2}$ and setting a maximum value of R_0 equal to 3 in case of no adoption on the left, and of 1.2 on the rigth. A solid red line indicates the threshold $R_0 = 1$, and the dashed black line the threshold line for the random adoption case.

4.3 Merging the three health intervention in random adoption

Up to now we studied the health intervention singularly, in this section we studied the early stage of a disease with all three health intervention with random adoption. First of all the approximation for the S compartment has to take into account all

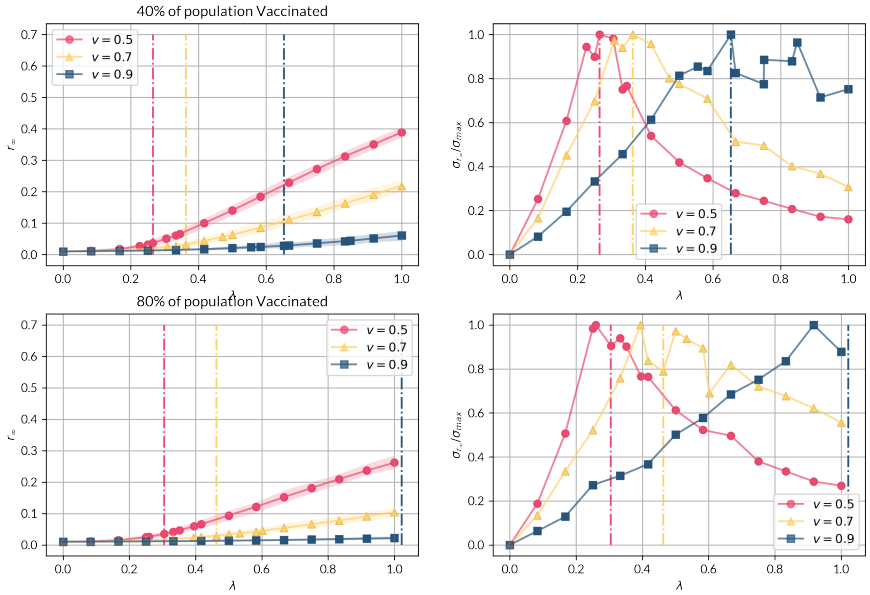

Figure 4.11: Vaccine activity based adoption phase transition plot with lower activity threshold. The plots display on the left the final epidemic size ($r_\infty = R_\infty/N$) with 95% confidence intervals for different values of λ and different values of effectiveness f in case of non-perfect adoption dependent on nodes' activity, with adopters **below** a certain activity threshold. The threshold is selected for different values of adoption f. Vertical dashed line indicates the analytical threshold derived from (4.60) with $f_< = 0$ and $f_> = 1$. The plots on the right display the normalized relative variance $\sigma_{r_\infty}/\sigma^{max}_{r_\infty}$ as a function of λ. The plots on the first line refer to the case with 40% of adoption, while in the second line to the case with 80% of adoption. Results are obtained by 10^2 stochastic simulation for each point and with the following model parameters: $\mu = 10^{-2}$, $N = 10^5$, $m = 2$, $i_0 = I_0/N = 0.01$ (initial fraction of infected seeds), while for the power law distribution the minimum value $\epsilon = 10^{-3}$, maximum equal to 1, and characteristic power $\alpha = 2.1$

the previously seen approximation

$$S_a^t \sim N_a^t - R_a^t = N_a^t - v f_u N_a^t = (1 - vf) N_a^t \tag{4.61}$$

The combination of the three health intervention gives birth to $2^3 \times 2^3 = 64$ possible type of combinations of infected-susceptible meeting. These luckily can be grouped

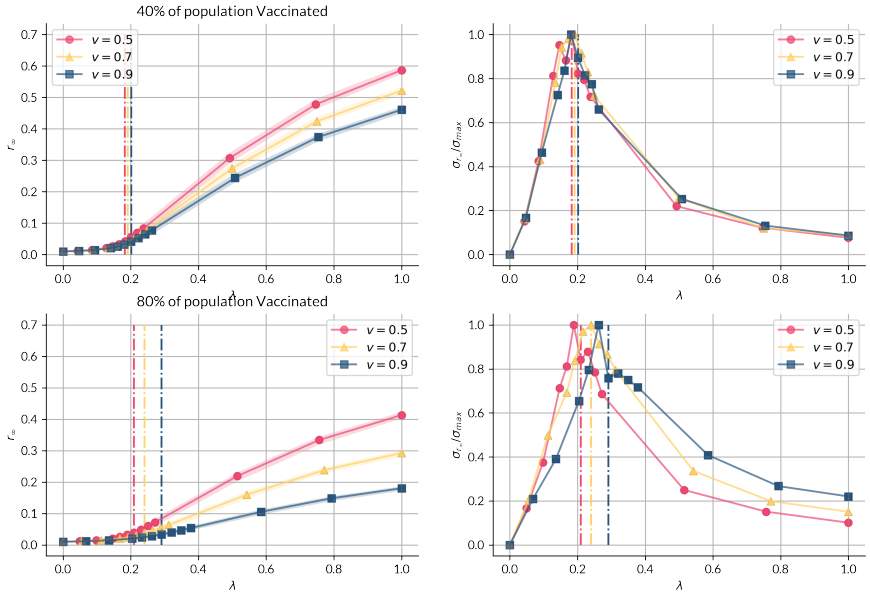

Figure 4.12: Vaccine activity based adoption phase transition plot with upper activity threshold. The plots display on the left the final epidemic size ($r_\infty = R_\infty/N$) with 95% confidence intervals for different values of λ and different values of effectiveness f in case of non-perfect adoption dependent on nodes' activity, with adopters **above** a certain activity threshold. The threshold is selected for different values of adoption f. Vertical dashed line indicates the analytical threshold derived from (4.60) with $f_< = 1$ and $f_> = 0$. The plots on the right display the normalized relative variance $\sigma_{r_\infty}/\sigma^{max}_{r_\infty}$ as a function of λ. The plots on the first line refer to the case with 40% of adoption, while in the second line to the case with 80% of adoption. The remaining parameters are settled as in the previous figure.

and give for the infected dynamics

$$I_a^{t+\Delta t} = I_a^t - \mu \Delta t I_a^t + (1-vf)\alpha_s \alpha_i \lambda m \psi_w \Delta t a N_a^t \int da \frac{I_a^t}{N} + \\ + (1-vf)\alpha_s \alpha_i \lambda m \gamma_p \Delta t N_a^t \int da \frac{a I_a^t}{N} \tag{4.62}$$

Developing the calculation this give to a threshold value R_0 equal to

$$\frac{\lambda}{\mu} > \frac{2}{m(1-vf)\alpha_s\alpha_i \langle a\rangle (\psi_w + \gamma_p) + m(1-vf)\alpha_s\alpha_i\sqrt{\langle a\rangle^2 (\psi_w - \gamma_p)^2 + 4\gamma_p\psi_w \langle a^2\rangle}} \tag{4.63}$$

$$R_0 = \frac{\lambda}{\mu}\frac{m(1-vf)\alpha_s\alpha_i \langle a\rangle (\psi_w + \gamma_p) + m(1-vf)\alpha_s\alpha_i\sqrt{\langle a\rangle^2 (\psi_w - \gamma_p)^2 + 4\gamma_p\psi_w \langle a^2\rangle}}{2} \tag{4.64}$$

Trying to turn off combination of health intervention it is possible to verify the rescue all the solution found up to now in random adoption.
It is also possible to combine different health interventions with activity based adoption, but being the terms this time with integrals, becomes not possible to easily group them. We verified that the procedure to find the threshold is not giving new challenges to the problem beyond that of patience in writing several repeating terms.
Despite this, the interplay of different health interventions remains of strong interest and this is what we have explored in the next chapter.

Chapter 5

Modeling the Interplay of Health Interventions on Activity Driven Network

5.1 Case study: Interplay of different behaviours above and below the activity threshold

In Ref. [29], as reported in chapter 3, has been simulated a scenario in which the more active population do not reduce their activity. This because that part of the population has the role of keep alive the daily life of the society, so more active individuals could be people working in hospitals, in distribution of basic necessities products.
After the study of the health intervention applied alone the question has been straightforward: what if the more active people, unable to reduce their activity, try to protect themselves and the whole population adopting another of the other health intervention.
In this case study we abandoned the study of the threshold to look at the effective evolution of a spreading in the population, recording and plotting the evolution of the compartments at every time-step.
The health intervention chosen for more active people are simulated singularly, so at every simulation less active population will experience activity reduction, while more active people will adopt three possible health intervention:

- use of face mask with random adoption
- vaccination with random adoption
- spotty use of face mask adoption

With first two health intervention already extensively covered during this thesis and the now introduced concept of spottiness.
The spotty use of face mask want to simulate the realistic scenario of people adopting the use of face mask but for various reasons (e.g. forgetfulness) with a certain rate do not wear it.
The concept of random adoption in this case study is combined with the one of activity based, in fact we decided to do not give a perfect adoption to people above the threshold but rather to try different percentage of random adoption above threshold.
In the previous chapters, each simulation stopped when no more infected nodes were in the population. In this case study the simulation all have a duration of 1000 time steps. The choice to stop before the effective end of the diffusion has the purpose of have the same time scale for all the simulation for better comparison, and after some attempt we noticed that at 1000 time steps the remaining infected were few and negligible for the evaluation of the total. It was also a good trade off between approximation and computing time.
The first scenario under study is the one with activity reduction $\gamma = \psi = 0.1$ for $p = w = 80\%$ of population under activity threshold and for the remaining 20% upper threshold to simulate different values of random adoption at 10%, 20%, 30%, 50%, 80% and 100% equal for infected and susceptible and an effectiveness of face mask of 20%.
In 5.4 we plotted the mean values with 95% C.I. of the infected fraction and of the total recovered fraction on the right for the six different cases. In the figure is plotted in dashed grey line also the case of 80% random adoption activity reduction, as expected way lower than the other cases. The simulation are repeated in the case that upper threshold population decide to get vaccinated, the fraction are the same and the chosen value for effectiveness of the vaccine is 70%. In figure 5.2 we report again the results for fraction of infected fraction and recovered fraction in function of time. We see the peak of the infected and the total recovered lower than the case of use of face mask and in the case of perfect adoption for the upper threshold to also go lower than the benchmark random adoption of activity reduction (always dashed grey line). The last case we introduced is the one with spottiness parameter.// A 100% spottiness is the equivalent of use of face mask, whom uses face mask always use. We decided to run simulations for three levels of spottiness:

- 20% of spottiness, to model population less aware to the health intervention
- 50% of spottiness, population uses face mask half of the times
- 70% of spottiness, population is aware to the use of face mask but sometimes not

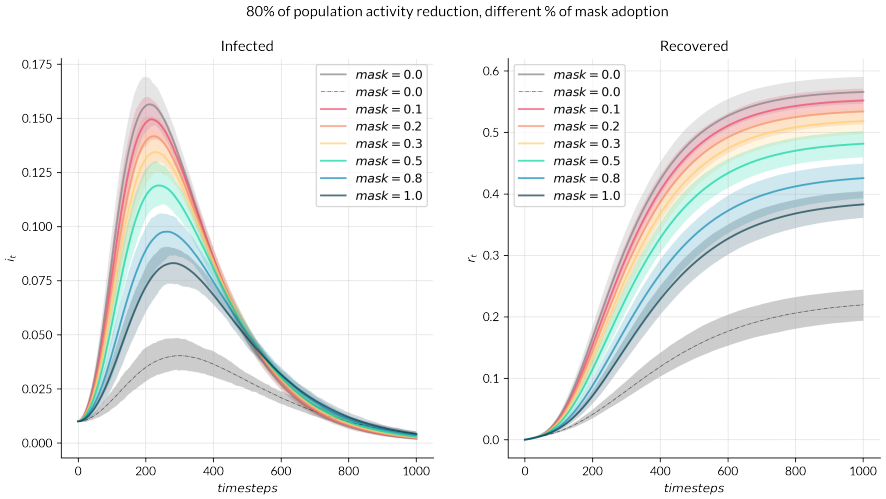

Figure 5.1: Interplay of activity reduction and use of face mask. Plot of the mean with 95% confidence interval of the infected fraction on the left and of recovered fraction on the right, in the case of 80% of population below activity threshold reducing their activity ($\gamma = \psi = 0.1$) with different levels of random face mask adoption for the 20% of population above threshold with effectiveness of 20% ($\alpha_m = 0.8$), in function of time. Results are obtained by 10^2 stochastic simulation for each point and with the following model parameters: time steps = 1000, $\mu = 10^{-2}$, $N = 10^5$, $m = 2$, $i_0 = I_0/N = 0.01$ (initial fraction of infected seeds), while for the power law distribution the minimum value $\epsilon = 10^{-3}$, maximum equal to 1, and characteristic power $\alpha = 2.1$. Grey dashed line corresponds to the activity reduction case with 80% random adoption

The three levels of spottiness have been simulated singularly and in figure 5.3 we plotted as in the previous cases the time evolution of infected fraction on the left, and om the right the time evolution of recovered fraction. As expected we can see how generally a greater level of spottiness reduce the spreading of the disease. In order to have a measure on how much higher levels of spottiness are better we evaluated the percent variation with respect to the no health intervention above threshold reference case. To do so we resampled this new metric through the method of bootstrapping: for every dataset formed of 100 simulations, we uniformly pick 1 of them and evaluate the percent difference with one of the uniformly picked from the reference case. This process is repeated 1000 times generating a sample for the estimate.
We focus on the total infected fraction percent variation. The total infected fraction is evaluated as the sum of infected fraction plus the recovered fraction at last time step. In figure 5.4 we box-plot the samples generated with bootstrapping, seeing

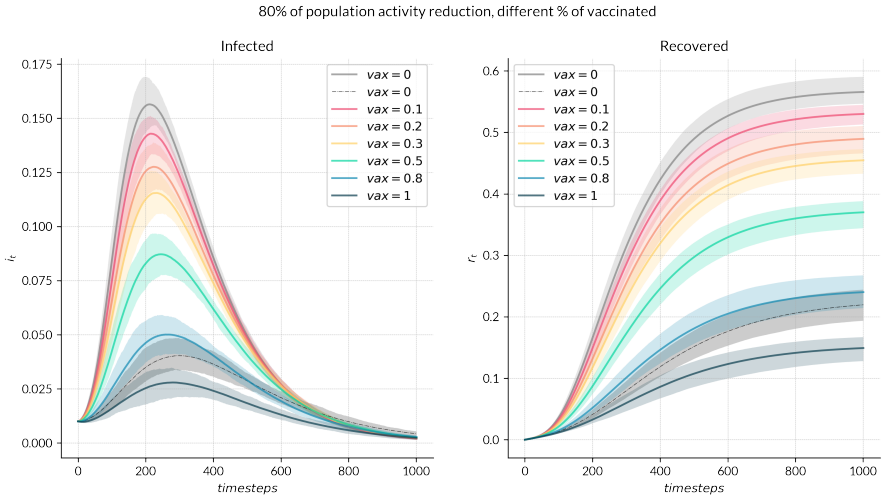

Figure 5.2: Interplay of activity reduction and vaccination. Plot of the mean with 95% confidence interval of the infected fraction on the left and of recovered fraction on the right, in the case of 80% of population below activity threshold reducing their activity ($\gamma = \psi = 0.1$) with different levels of random vaccine adoption for the 20% of population above threshold with effectiveness v of 70%, in function of time. Results are obtained by 10^2 stochastic simulation for each point and with the following model parameters: time steps = 1000, $\mu = 10^{-2}$, $N = 10^5$, $m = 2$, $i_0 = I_0/N = 0.01$ (initial fraction of infected seeds), while for the power law distribution the minimum value $\epsilon = 10^{-3}$, maximum equal to 1, and characteristic power $\alpha = 2.1$. Grey dashed line corresponds to the activity reduction case with 80% random adoption

how the reduction for small adoption is similar through different levels of spottiness, but then at increasing adoption corresponds a marked separation with higher levels of spottiness experiencing higher reductions. The same method described for the total infected fraction percent reduction is applied to evaluate the reduction of the peak of infection with respect to the case with no adoption in 5.5 We decided to sample the two metrics with bootstrapping also for the vaccine simulations and produce a comparison with face mask (100% spottiness) and 20% spottiness box-plots. In figure 5.6 the comparison for the fraction of infected percent reduction, and in figure 5.6 the percent reduction of peak of infected.
As expected the vaccination campaign has better results in mitigating the spread of infection, almost doubling the reduction of peak and total infected with respect the use of face mask.

5.2 Case study: Interplay of different behaviours above and below the activity threshold

In the previous section we studied the interplay of two different health intervention at a time for each simulation, but no individual choose to adopt both of them, the two set were totally disjoint. In real world population is common the scenario in which who wants to protect himself adopts more than one single health intervention. Reasoning about this scenario suggest the introduction of a new parameter: the overlap of adopters.
Now we imagine a scenario in which two health intervention have an equal fraction of adopters, and the overlap parameters is a fraction of how many of them adopts both the health intervention. The adopters fraction is a number between zero and one, while the overlap fraction needs to respect the condition (5.2)

$$0 \leq 2\,adopters - adopters \times overlap \leq 1 \tag{5.1}$$

$$1 \geq overlap \geq 2 - \frac{1}{adopters} \tag{5.2}$$

The first two health intervention under test are vaccination and activity reduction, the effectiveness of vaccine is 70% and the reductions are 90% for infected ($\gamma = 0.1$) and 20% for the susceptible ($\psi = 0.8$). The values of adopters are 20%, 50% and 65%, and are combined with values of overlap of 0%, 25%, 50%, 75% and 100%. We ran again 100 simulations for 1000 time step for each possible combination, in figure 5.8 we plotted the infected fraction on the left and the recovered fraction evolving in time. Notice that the case with 65% adopters only presents the lines with overlap values great or equal to 50%, because of the (5.2) condition. To evaluate the variation percent of total infected we execute again the bootstrapping taking as a reference the 100%overlap case for each adoption. This produced the box-plot in figure 5.9 showing how the greater the overlap the worst for the population. Meaning of also if part of the population adopts strict conditions to prevent diffusion, the opposition of individuals not adopting health intervention will punish the entire population. In figure 5.10 we repeated the bootstrapping for the percent variation of the peak of infection, showing again how total disjunction of groups is a better option Adding some other simulation, in particular in the case of 35%, 80% and 100% adopters with the relative possible overlap value, and bootstrapping all with respect to the no health intervention case, we plotted two color-map in figure 5.11 for the percentage variation of total infected and of the percentage variation of peak of infection with respect to the no health intervention case. The color-map shows how the reduction grows with adoption while decrease with overlap, both for total infection and peak of infection.

We also replicated this experiment substituting at the activity reduction the

use of face mask with effectiveness of 20%. The other parameters remain the same, and in figure 5.12 we reported the infected and recovered fractions plot as made in the previous case. And again the percent variation of total infected and of the peak of infected in figures 5.13 and 5.14 conforming also for the vaccination-face mask scenario the collaborative behaviour rewards the entire population. We ran the simulation for the other three values of adoption as in the previous case and reported also for the interplay of vaccine and face mask the generated color-map in figure 5.15

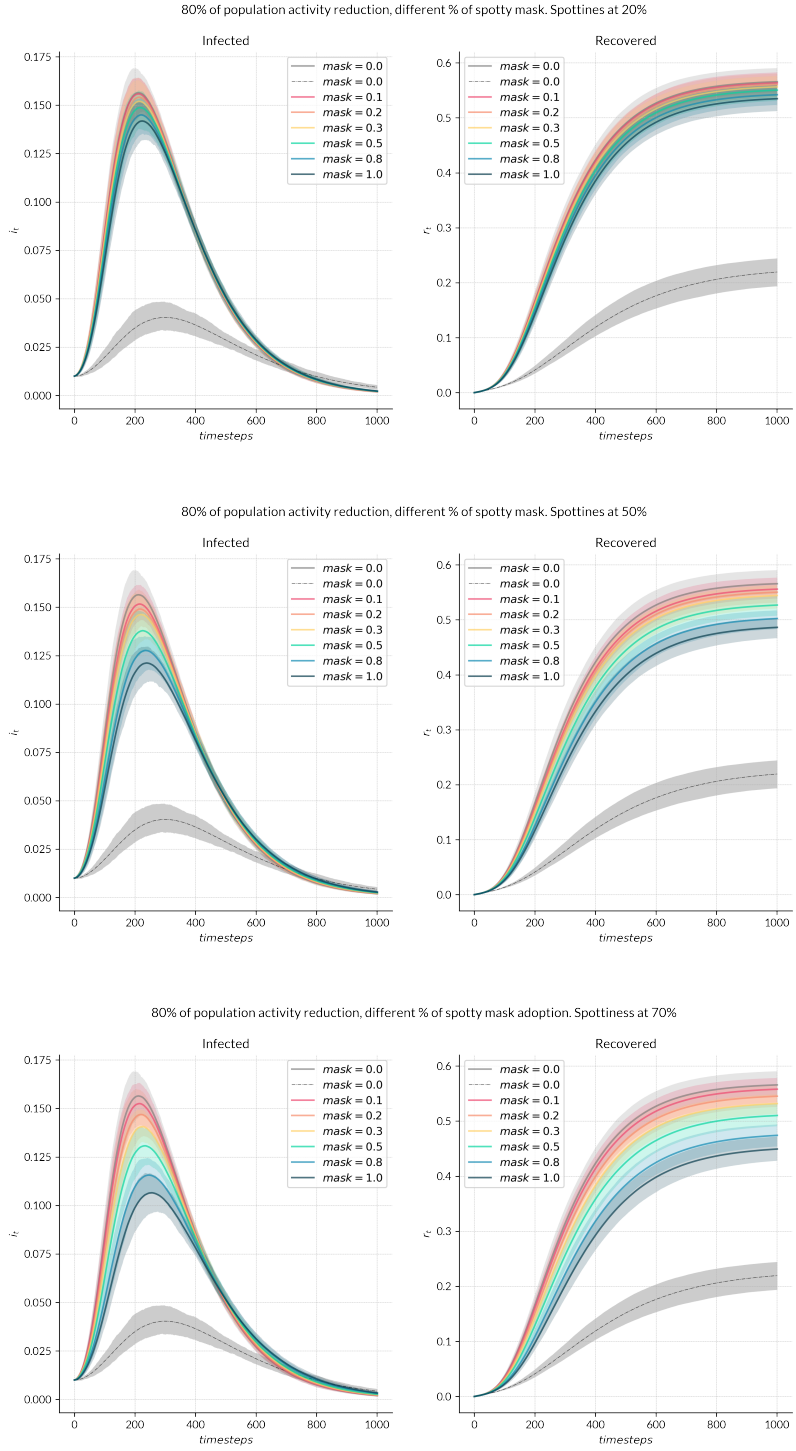

Figure 5.3: Interplay of activity reduction and face mask adoption with different levels of spottiness. Plot of the mean with 95% confidence interval of the infected fraction on the left and of recovered fraction on the right, in the case of 80% of population below activity threshold reducing their activity ($\gamma = \psi = 0.1$) with different levels of random face mask adoption for the 20% of population above threshold with effectiveness of 20% ($\alpha_m = 0.8$), in function of time. The first line presents a spottiness level of 20%, the second of 50% and the third of 70%. Results are obtained by 10^2 stochastic simulation for each point and with the following model parameters: time steps = 1000, $\mu = 10^{-2}$, $N = 10^5$, $m = 2$, $i_0 = I_0/N = 0.01$ (initial fraction of infected seeds), while for the power law distribution the minimum value $\epsilon = 10^{-3}$, maximum equal to 1, and characteristic power $\alpha = 2.1$. Grey dashed line corresponds to the activity reduction case with 80% random adoption

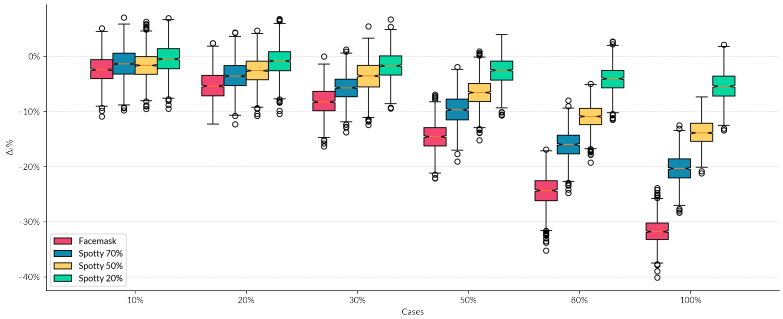

Figure 5.4: Variation percent of total infected with different levels of spottiness. Knot plot of percent variation of the total infection ($i_{1000} + r_{1000}$). Each knot plot is generated bootstrapping 1000 with respect the 0% adoption. Data used for the bootstrapping are taken from the 100 simulations of the spotty case

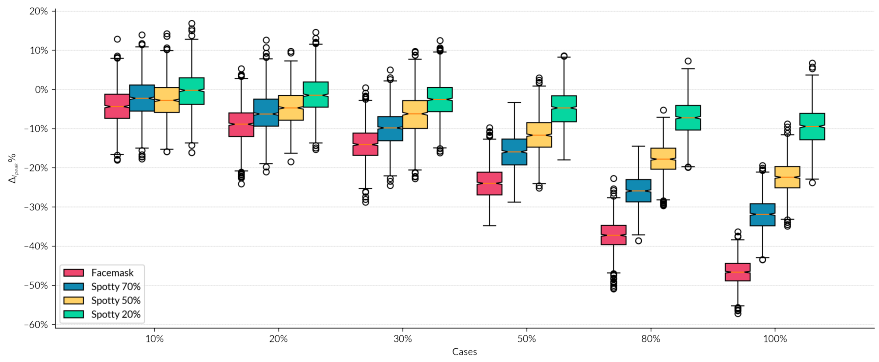

Figure 5.5: Variation percent of the peak infected with different levels of spottiness. Knot plot of percent variation of the peak of infection. Each knot plot is generated bootstrapping 1000 with respect the 0% adoption. Data used for the bootstrapping are taken from the 100 simulations of the spotty case

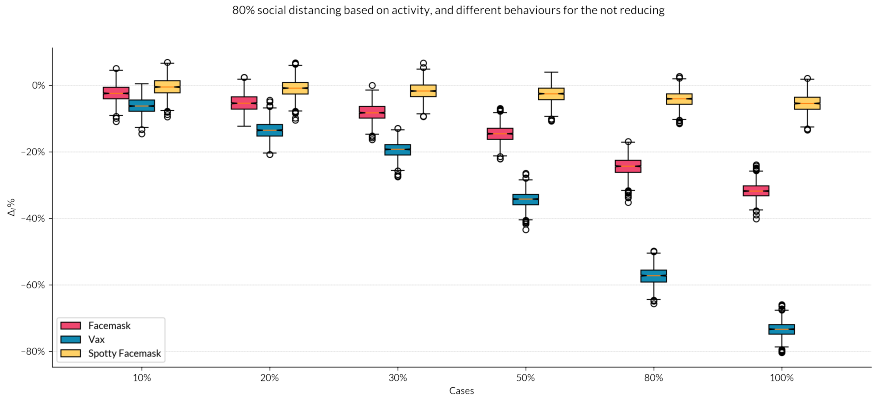

Figure 5.6: Variation percent of total infected with different health intervention. Knot plot of percent variation of the total infection $(i_{1000} + r_{1000})$ for the three health intervention: face mask, vaccination spotty face mask at 20%. Each knot plot is generated bootstrapping 1000 with respect the 0% adoption. Data used for the bootstrapping are taken from the previous simulations

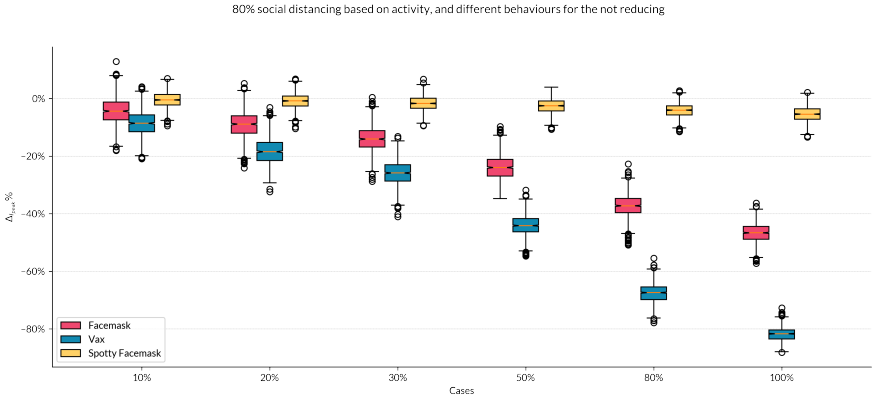

Figure 5.7: Variation percent of the peak of infected with different health intervention. Knot plot of percent variation of the peak of infection for the three health interventions: face mask, vaccination spotty face mask at 20%. Each knot plot is generated bootstrapping 1000 with respect the 0% adoption. Data used for the bootstrapping are taken from the previous simulations

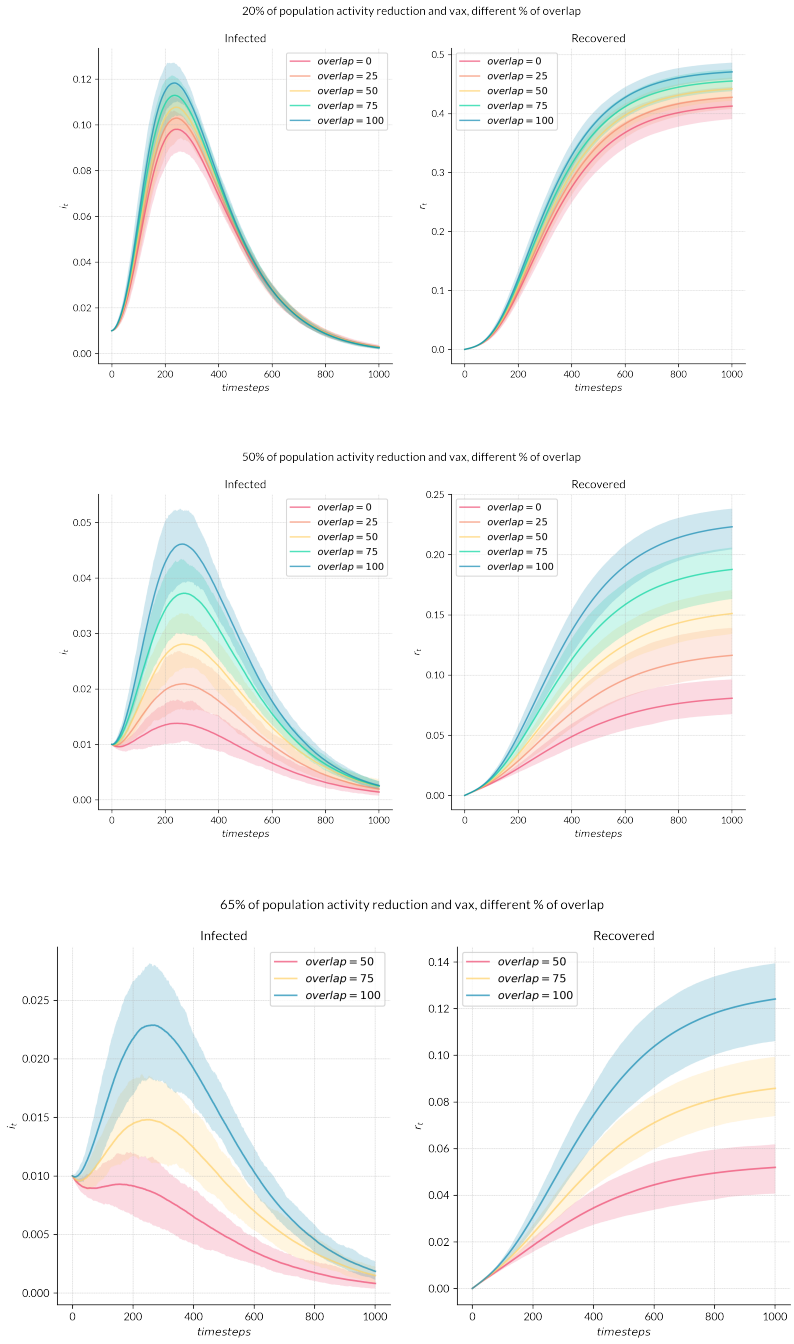

Figure 5.8: Interplay of activity reduction and vaccination with different levels of adoption and overlap. Plot of the mean with 95% confidence interval of the infected fraction on the left and of recovered fraction on the right, for 3 different levels of adoption and different values of overlap in the case of random adoption of activity reduction ($\psi = \gamma = 0.1$) and vaccination ($v = 0.7$), in function of time. The first line presents an adoption of 20%, the second of 50% and the third of 65%. Results are obtained by 10^2 stochastic simulation for each point and with the following model parameters: time steps = 1000, $\mu = 10^{-2}$, $N = 10^5$, $m = 2$, $i_0 = I_0/N = 0.01$ (initial fraction of infected seeds), while for the power law distribution the minimum value $\epsilon = 10^{-3}$, maximum equal to 1, and characteristic power $\alpha = 2.1$.

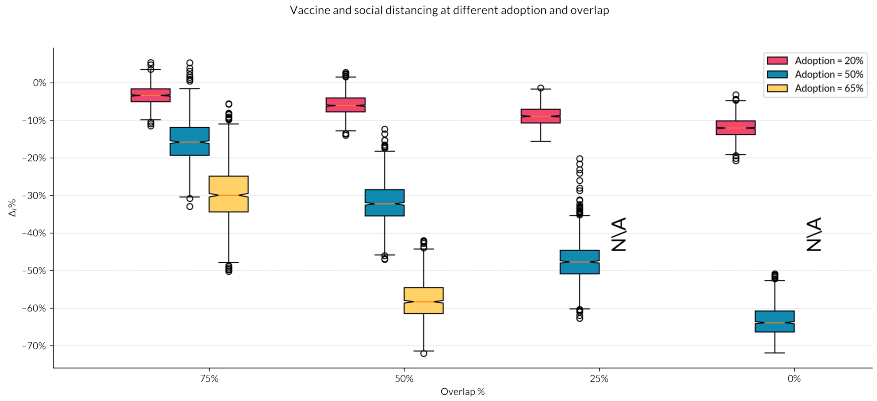

Figure 5.9: Variation percent of total infected with different levels of adoption and overlap of activity reduction and vaccination. Knot plot of percent variation of the total infection ($i_{1000} + r_{1000}$) for the three levels of adoption: 20%, 50% and 65% for each level of overlap of overlap social distancing and vaccine adopters. Each knot plot is generated bootstrapping 1000 data points with respect to the 100% overlap. Data used for the bootstrapping are taken from the previous simulations. Not available data because of the n=1 condition

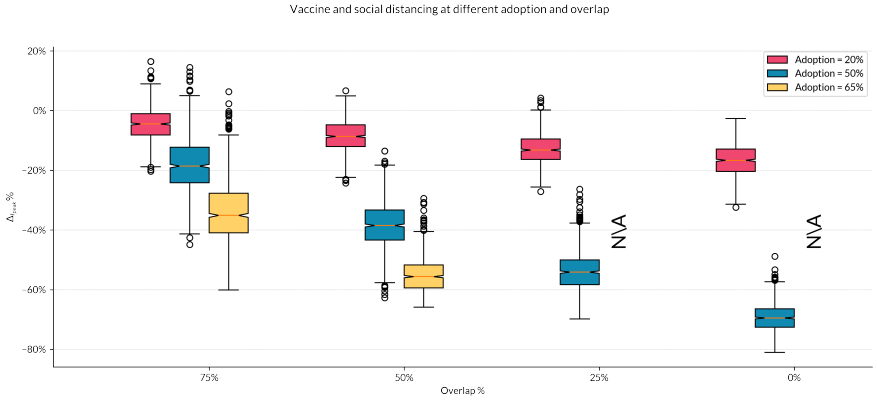

Figure 5.10: Variation percent of the peak of infected with different levels of adoption and overlap of activity reduction and vaccination. Knot plot of percent variation of the peak of infection for the three levels of adoption: 20%, 50% and 65% for each level of overlap of overlap social distancing and vaccine adopters. Each knot plot is generated bootstrapping 1000 data points with respect to the 100% overlap. Data used for the bootstrapping are taken from the previous simulations. Not available data because of the n=1 condition

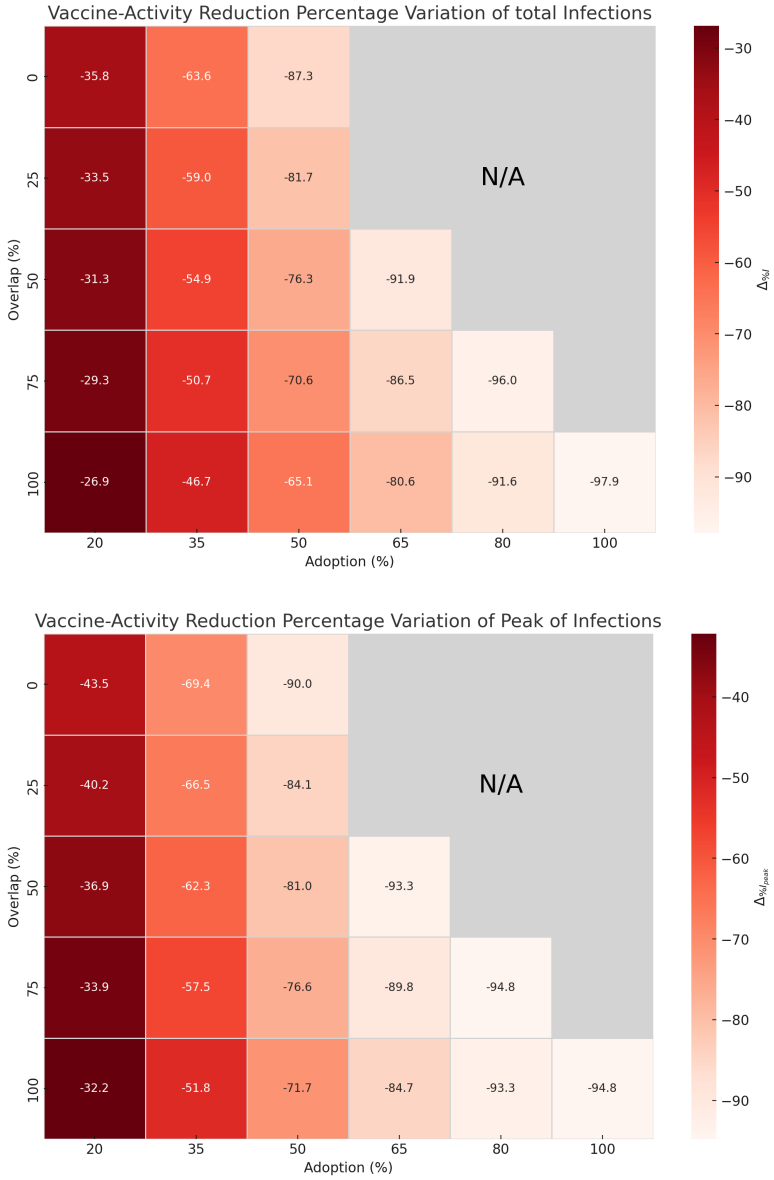

Figure 5.11: Color-map of total infected percent variation and for peak variation for activity reduction and vaccination with different levels of adoption and overlap. The values in the color-map are the median value of the total infected variation in the first plot and of the peak of infection variation in the second infection, both as function of different values overlap and of adoption of social distancing and vaccine adopters. Each knot plot is generated bootstrapping 1000 data points with respect to the 0% adoption. Data used for the bootstrapping are taken from the previous simulations. Not available data because of the n=1 condition

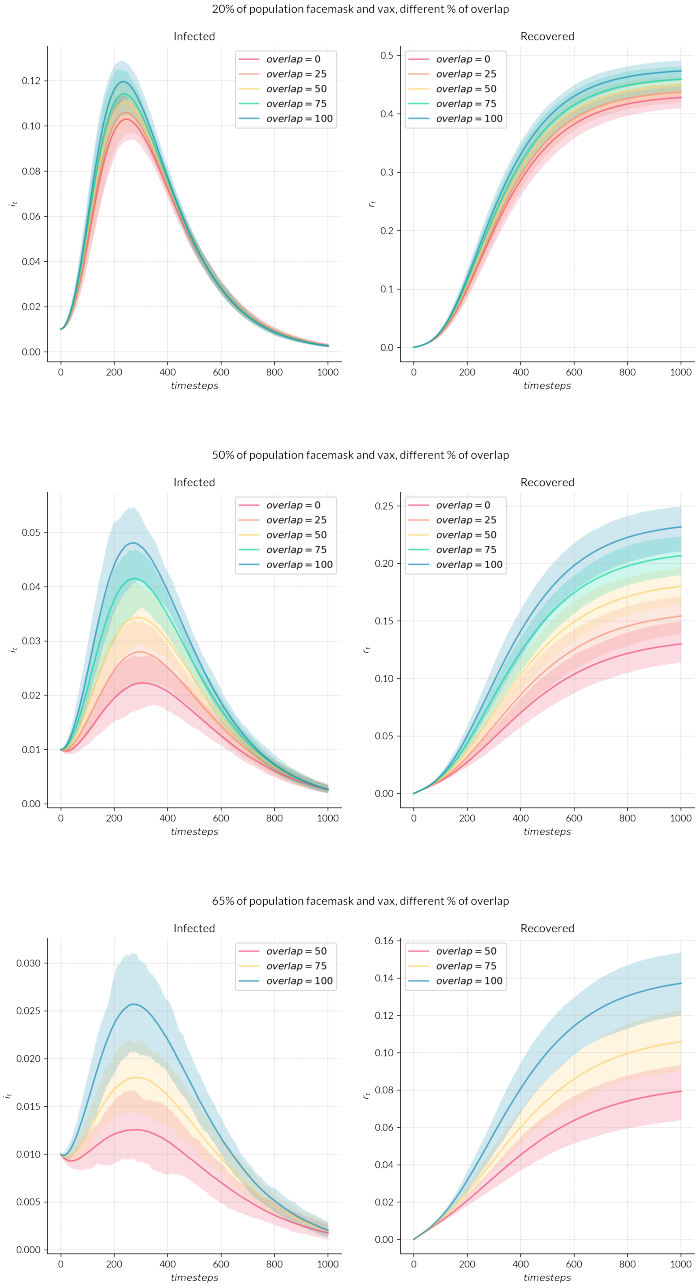

Figure 5.12: Interplay of activity reduction and vaccination with different levels of adoption and overlap. Plot of the mean with 95% confidence interval of the infected fraction on the left and of recovered fraction on the right, for 3 different levels of adoption and different values of overlap in the case of random adoption of face mask ($\alpha_m = 0.8$) and vaccination ($v = 0.7$), in function of time. The first line presents an adoption of 20%, the second of 50% and the third of 65%. Results are obtained by 10^2 stochastic simulation for each point and with the following model parameters: time steps $= 1000$, $\mu = 10^{-2}$, $N = 10^5$, $m = 2$, $i_0 = I_0/N = 0.01$ (initial fraction of infected seeds), while for the power law distribution the minimum value $\epsilon = 10^{-3}$, maximum equal to 1, and characteristic power $\alpha = 2.1$.

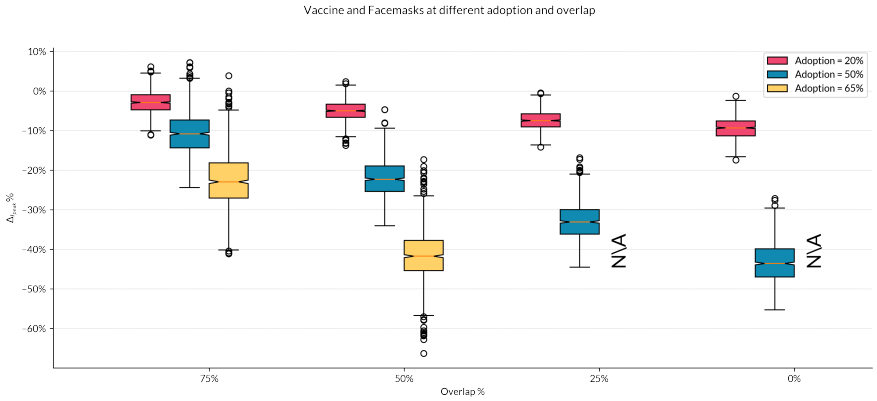

Figure 5.13: Variation percent of total infected with different levels of adoption and overlap of use of face mask and vaccination. Knot plot of percent variation of the total infection ($i_{1000} + r_{1000}$) for the three levels of adoption: 20%, 50% and 65% for each level of vaccine and face mask adopters. Each knot plot is generated bootstrapping 1000 data points with respect to the 100% overlap. Data used for the bootstrapping are taken from the previous simulations. Not available data because of the n=1 condition

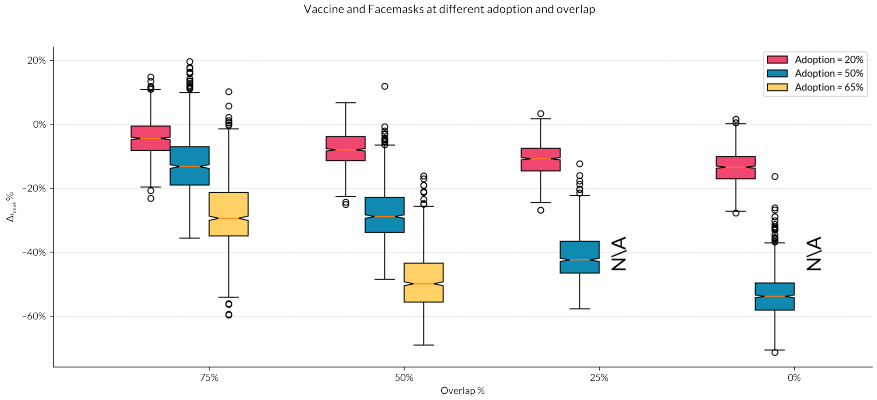

Figure 5.14: Variation percent of the peak of infected with different levels of adoption and overlap of use of face mask reduction and vaccination. Knot plot of percent variation of the peak of infection for the three levels of adoption: 20%, 50% and 65% for each level of vaccine and face mask adopters. Each knot plot is generated bootstrapping 1000 data points with respect to the 100% overlap. Data used for the bootstrapping are taken from the previous simulations. Not available data because of the n=1 condition

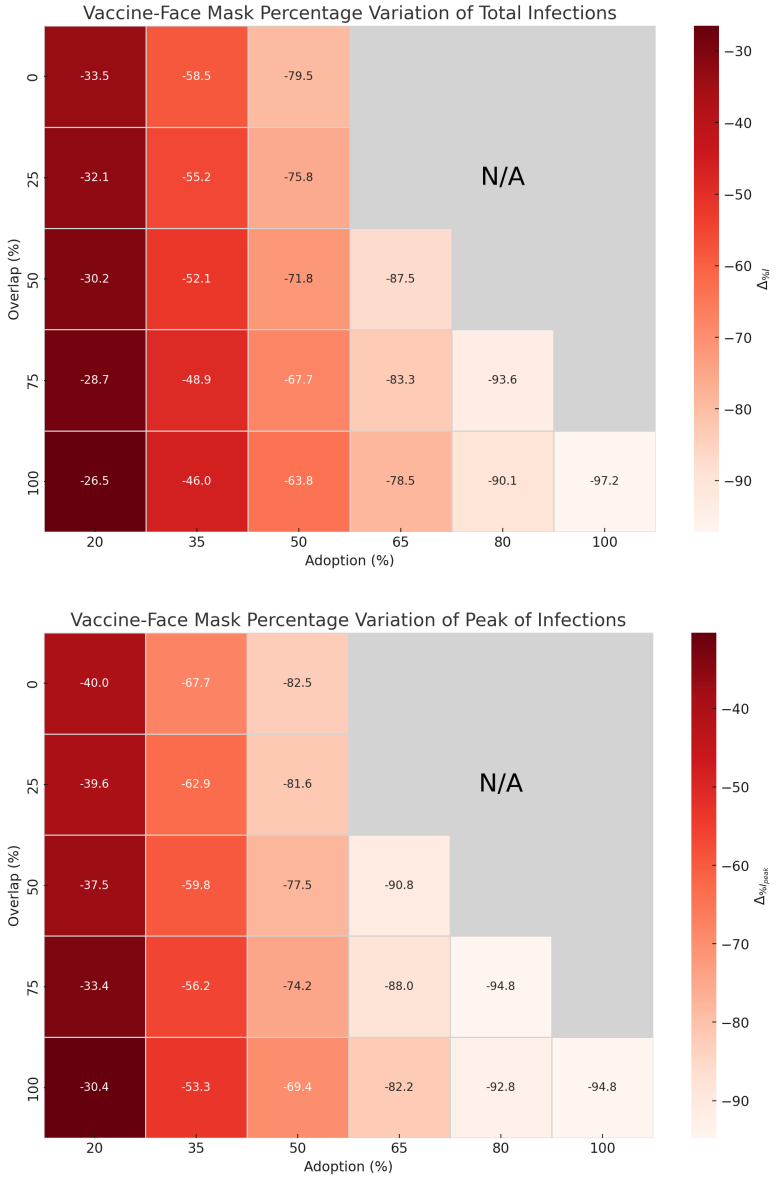

Figure 5.15: Color-map of total infected percent variation and for peak variation for face mask and vaccination with different levels of adoption and overlap. The values in the color-map are the median value of the total infected variation in the first plot and of the peak of infection variation in the second infection, both as function of different values overlap and of adoption of face mask and vaccine adopters. Each knot plot is generated bootstrapping 1000 data points with respect to the 0% adoption. Data used for the bootstrapping are taken from the previous simulations. Not available data because of the n=1 condition

Chapter 6

Conclusion

This thesis aims to contribute to effective pandemic modeling by incorporating modern concepts from social network theory and integrating health interventions into epidemic contexts. Starting with traditional models, we progressively relaxed various assumptions to develop more realistic and sophisticated models. It is noteworthy that we derived analytical solutions to complex problems and validated these solutions.

The term "health intervention" has been intentionally used throughout this work because the concept of "behavioral change" inherently includes feedback loops. These feedback loops can be implemented by appropriately modifying compartments and their transitions within the models. During the modeling process, these feedback loops successfully demonstrated some of the dynamics observed in pandemic data, such as the emergence of multiple waves of infections driven by changes in individual behavior within networks.

Exploring the relaxation of assumptions can take multiple directions. One straightforward approach is to introduce the concept of communities, thereby incorporating correlation into the network and moving away from the unrealistic assumption of a completely uncorrelated network. It is particularly interesting to observe the effects when individuals within the same community adopt health interventions, creating modularity in both the network and intervention adoption.

Another promising direction for future research is the integration of real-world data into the models. Depending on the type of data, it could be used to calibrate the parameters of various health interventions, validate network dynamics, and enable individual or class-specific parameterization. Making models data-driven is a significant opportunity, given the vast amount of data available. Historical data has shown the inadequacy of past models, and future models must leverage this data for validation and improvement.

Throughout the simulations, we tested several combinations of preventive measures, although many more combinations remain to be explored. Our findings underscore

the necessity of a collective effort to minimize the impact of pathogens, which will inevitably continue to affect future populations. Health interventions can play a crucial role in preparing for and mitigating the effects of potential future pandemics, similar to COVID-19. Moreover, understanding how health interventions influence the spread of endemic seasonal influenza could provide additional insights.

Appendix A

Sample from power law distribution

The chosen distribution in order to exploit heavy tail properties is the power law distribution, with power α

$$F(x) \propto x^{-\alpha} \tag{A.1}$$

In this case, the distribution is limited below by ϵ near to zero in order to avoid anomalous divergences in zero, and above by 1, as the variable to sample is a probability rate (the activity) and the time scale is arbitrary.
The distribution has to respect the sum 1 constraint, in this way it is possible to evaluate the proportionality constant of the distribution

$$\int_1^\epsilon F(x)\,dx = \int_1^\epsilon Cx^{-\alpha}\,dx = 1 \tag{A.2}$$

$$C = \frac{1-\epsilon^{1-\alpha}}{1-\alpha} \tag{A.3}$$

$$F(x) = \frac{1-\epsilon^{1-\alpha}}{1-\alpha}x^{-\alpha} \tag{A.4}$$

To randomly sample from this distribution, we exploit the inverse transformation method. In a continuous distribution, the cumulative distribution function (CDF) maps one-to-one with the 0-1 interval.
The CDF reads

$$CDF(x) = \frac{1-\epsilon^{1-\alpha}}{1-\alpha}\int_x^\epsilon x'^{-\alpha}\,dx' \tag{A.5}$$

$$CDF(x) = \frac{x^{1-\alpha}-\epsilon^{1-\alpha}}{1-\epsilon^{1-\alpha}} \tag{A.6}$$

Inverting the CDF and feeding it with pseudo-random numbers generated by a computer between 0 and 1 gives the random sample of the distribution.
Calling y the cumulative, the inverse reads

$$x = \left[1 - y\left(1 - \epsilon^{1-\alpha}\right)\right]^{\frac{1}{1-\alpha}} \tag{A.7}$$

Feeding y with random numbers, it is possible to sample from the power law distribution. In figure A.1, the sample for a distribution with $\alpha = 2.1$ and $\epsilon = 10^{-3}$ is shown on a log-log scale to highlight the heavy tail, which is not appreciated on a decimal scale.

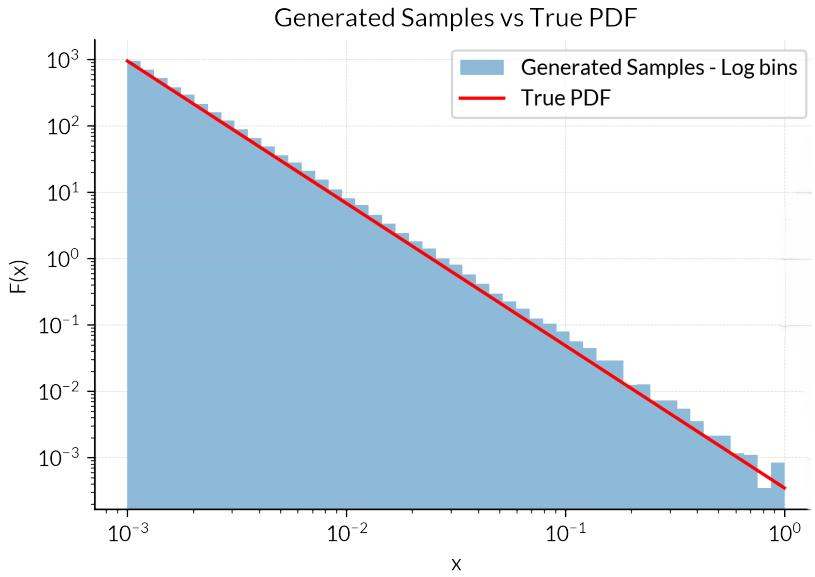

Figure A.1: Sampling from a power law distribution

Appendix B

Social distancing threshold analytical solution

B.0.1 Random Adoption

Starting from (3.28)

$$I_a^{t+\Delta t} = I_a^t - \mu \Delta t I_a^t + \lambda m \Delta t a N_a^t \psi_w \int da \frac{I_a^t}{N} + \lambda m \Delta t N_a^t \gamma_p \int da \frac{a I_a^t}{N} \tag{B.1}$$

Integrate in $\int da$ and taking the continuous limit

$$\partial_t I^t = -\mu I^t + \lambda m \psi_w \langle a \rangle I^t + \lambda m \gamma_p \Theta^t \tag{B.2}$$

and the equation for Θ^t after integrating $\int da\, a$ and taking the continuous limit

$$\partial_t \Theta^t = -\mu \Theta^t + \lambda m \psi_w \left\langle a^2 \right\rangle I^t + \lambda m \gamma_p \langle a \rangle \Theta^t \tag{B.3}$$

Matrix representation of the system

$$\begin{bmatrix} \partial_t I^t \\ \partial_t \Theta^t \end{bmatrix} = \begin{bmatrix} -\mu + \lambda m \psi_w \langle a \rangle & \lambda m \gamma_p \\ \lambda m \psi_w \langle a^2 \rangle & -\mu + \lambda m \gamma_p \langle a \rangle \end{bmatrix} \begin{bmatrix} I^t \\ \Theta^t \end{bmatrix}$$

Solve $det(J - I\Lambda) = 0$

$$(-\mu + \lambda m\psi_w \langle a\rangle - \Lambda)(-\mu + \lambda m\gamma_p \langle a\rangle - \Lambda) - (\lambda m\gamma_p)(\lambda m\psi_w \left\langle a^2\right\rangle) = 0 \quad \text{(B.4)}$$

$$\Lambda^2 + [2\mu - \lambda m \langle a\rangle (\psi_w + \gamma_p)]\Lambda +$$
$$[\lambda^2 m^2 \psi_w \gamma_p (\langle a\rangle^2 - \left\langle a^2\right\rangle) + \mu^2 - \mu\lambda m(\psi_w + \gamma_p)] = 0 \quad \text{(B.5)}$$

$$b^2 - 4ac = \lambda^2 m^2 \langle a\rangle^2 (\psi_w + \gamma_p)^2 - 4\lambda^2 m^2 \gamma_p \psi_w (\langle a\rangle^2 - \left\langle a^2\right\rangle) =$$
$$= \lambda^2 m^2 \langle a\rangle^2 (\psi_w - \gamma_p)^2 - 4\lambda^2 m^2 \gamma_p \psi_w \left\langle a^2\right\rangle \quad \text{(B.6)}$$

$$\Lambda_{(1,2)} = \frac{1}{2}[2\mu - \lambda m \langle a\rangle (\psi_w + \gamma_p) \pm \lambda m\sqrt{\langle a\rangle^2 (\psi_w - \gamma_p)^2 - 4\gamma_p \psi_w \langle a^2\rangle}] \quad \text{(B.7)}$$
$$\Lambda > 0$$

$$\frac{\lambda}{\mu} > \frac{2}{m \langle a\rangle (\psi_w + \gamma_p) + m\sqrt{\langle a\rangle^2 (\psi_w - \gamma_p)^2 + 4\gamma_p \psi_w \langle a^2\rangle}} \quad \text{(B.8)}$$

$$R_0 = \frac{\lambda}{\mu} \frac{m \langle a\rangle (\psi_w + \gamma_p) + m\sqrt{\langle a\rangle^2 (\psi_w - \gamma_p)^2 + 4\gamma_p \psi_w \langle a^2\rangle}}{2} > 1 \quad \text{(B.9)}$$

Obtaining the result of (3.29)

B.0.2 Activity Based Adoption

Starting from equation (3.33)

$$I_a^{t+\Delta t} = I_a^t - \mu \Delta t I_a^t + \lambda m \Delta t a \left[1 + (\psi - 1)H(u_s - a)\right] N_a^t \int da \frac{I_a^t}{N} +$$
$$+ \lambda m \Delta t N_a^t \int da \left[1 + (\gamma - 1)H(u_i - a)\right] \frac{a I_a^t}{N} \quad \text{(B.10)}$$

Integrate in $\int da$ both sides

$$\begin{aligned}\int daI_a^{t+\Delta t} &= \int daI_a^t - \mu\Delta t \int daI_a^t + \\ &+ \lambda m\Delta t \int daa(1+(\psi-1)H(m-a))N_a \int da' \frac{I_{a'}^t}{N} + \\ &+ \lambda m\Delta t \int daN_a \int da'(1+(\gamma-1)H(n-a'))\frac{aI_{a'}^t}{N} \qquad \text{(B.11)} \\ &= I^t - \mu\Delta t I^t + \lambda m\Delta t(\psi \langle a\rangle_{\epsilon,m} + \langle a\rangle_{m,1})I^t + \lambda m\Delta t\Theta^t \qquad \text{(B.12)}\end{aligned}$$

where

$$\Theta^t = \int da'(1+(\gamma-1)H(n-a'))\frac{aI_{a'}^t}{N} \qquad \text{(B.13)}$$

For the equation for Θ^t, integrate in $\int da\, a(1+(\gamma-1)H(n-a))$

$$\begin{aligned}\int da(1+(\gamma-1)H(n-a))aI_a^{t+\Delta t} &= \int da(1+(\gamma-1)H(n-a))aI_a^t - \qquad 2005/06/28ve \\ &\mu\Delta t \int da(1+(\gamma-1)H(n-a))aI_a^t + \\ &\lambda m\Delta t \int da(1+(\gamma-1)H(n-a))a^2N_a^t \int da' \frac{I_{a'}^t}{N} + \\ &\lambda m\Delta t \int da(1+(\gamma-1)H(n-a))aN_a^t \int da' \frac{aI_{a'}^t}{N} \qquad \text{(B.14)} \\ \Theta^{t+\Delta t} &= \Theta^t - \mu\Delta t\Theta^t + \lambda m\Delta t(\psi\gamma \left\langle a^2\right\rangle_{\epsilon,m} + \gamma \left\langle a^2\right\rangle_{m,n} + \left\langle a^2\right\rangle_{n,1})I^t + \\ &\lambda m\Delta t(\gamma \langle a\rangle_{\epsilon,n} + \langle a\rangle_{n,1})\Theta^t \qquad \text{(B.15)}\end{aligned}$$

taking the continuous limit

$$\partial_t\Theta^t = -\mu\Theta^t + \lambda m(\psi\gamma \left\langle a^2\right\rangle_{\epsilon,m} + \gamma \left\langle a^2\right\rangle_{m,n} + \left\langle a^2\right\rangle_{n,1})I^t + \lambda m(\gamma \langle a\rangle_{\epsilon,n} + \langle a\rangle_{n,1})\Theta^t \qquad \text{(B.16)}$$

Solve the system of differential equations with Jacobi matrix, the epidemic threshold is obtained when the greatest eigenvalue is larger than zero

$$\begin{bmatrix}\partial_t I^t \\ \partial_t\Theta^t\end{bmatrix} = \begin{bmatrix}-\mu + \lambda m(\psi \langle a\rangle_{\epsilon,m} + \langle a\rangle_{m,1}) & \lambda m \\ \lambda m(\psi\gamma \langle a^2\rangle_{\epsilon,m} + \gamma \langle a^2\rangle_{m,n} + \langle a^2\rangle_{n,1}) & -\mu + \lambda m(\gamma \langle a\rangle_{\epsilon,n} + \langle a\rangle_{n,1})\end{bmatrix}\begin{bmatrix}I^t \\ \Theta^t\end{bmatrix}$$

Solve $det(J - I(\frac{\Lambda' - \mu}{\lambda m}) = 0$
$\Lambda = \frac{\Lambda' - \mu}{\lambda m}$

$$((\psi \langle a \rangle_{\epsilon,m} + \langle a \rangle_{m,1}) - \Lambda)((\gamma \langle a \rangle_{\epsilon,n} + \langle a \rangle_{n,1}) - \Lambda) - (\psi\gamma \left\langle a^2 \right\rangle_{\epsilon,m} + \gamma \left\langle a^2 \right\rangle_{m,n} + \left\langle a^2 \right\rangle_{n,1}) = 0 \tag{B.17}$$

$$\Lambda^2 + [(\psi \langle a \rangle_{\epsilon,m} + \langle a \rangle_{m,1} + (\gamma \langle a \rangle_{\epsilon,n} + \langle a \rangle_{n,1})]\Lambda + \\ + [(\psi \langle a \rangle_{\epsilon,m} + \langle a \rangle_{m,1})(\gamma \langle a \rangle_{\epsilon,n} + \langle a \rangle_{n,1}) - (\psi\gamma \left\langle a^2 \right\rangle_{\epsilon,m} + \gamma \left\langle a^2 \right\rangle_{m,n} + \left\langle a^2 \right\rangle_{n,1})] = 0 \tag{B.18}$$

$$b^2 - 4ac = [(1 - \psi) \langle a \rangle_{\epsilon,m} - (1 - \gamma) \langle a \rangle_{\epsilon,n}]^2 - 4[(\psi - 1)\gamma \left\langle a^2 \right\rangle_{\epsilon,m} + (\gamma - 1) \left\langle a^2 \right\rangle_{\epsilon,n} + 1] \tag{B.19}$$

writing the determinant as

$$\mathcal{F}(u_s, \psi, u_i, \gamma) = [(1 - \psi) \langle a \rangle_{\epsilon,u_s} - (1 - \gamma) \langle a \rangle_{\epsilon,u_i}]^2 - \\ + 4[(\psi - 1)\gamma \left\langle a^2 \right\rangle_{\epsilon,u_s} + (\gamma - 1) \left\langle a^2 \right\rangle_{\epsilon,u_i} + 1] \tag{B.20}$$

$$\Lambda_{(1,2)} = \frac{1}{2}[2 + (\psi - 1) \langle a \rangle_{\epsilon,m} - (\gamma - 1) \langle a \rangle_{\epsilon,n} \pm \lambda m \sqrt{\mathcal{F}(u_s, \psi, u_i, \gamma)}] \tag{B.21}$$
$\Lambda > 0$

recovering the result of (3.35)

$$\frac{\lambda}{\mu} > \frac{2/m}{2 + (\psi - 1) \langle a \rangle_{\epsilon,u_s} - (\gamma - 1) \langle a \rangle_{\epsilon,u_i} + \lambda m \sqrt{\mathcal{F}(u_s, \psi, u_i, \gamma)}} \tag{B.22}$$

$$R_0 = \frac{\lambda m}{\mu} \frac{2 + (\psi - 1) \langle a \rangle_{\epsilon,u_s} - (\gamma - 1) \langle a \rangle_{\epsilon,u_i} + \lambda m \sqrt{\mathcal{F}(u_s, \psi, u_i, \gamma)}}{2} > 1 \tag{B.23}$$

Bibliography

[1] R. J. Littman and M. L. Littman. «Galen and the Antonine Plague». In: *The American Journal of Philology* 94.3 (1973), pp. 243–255. ISSN: 00029475, 10863168. URL: http://www.jstor.org/stable/293979 (visited on 06/24/2024) (cit. on p. 1).

[2] J. Haldon, Hugh Elton, Sabine Huebner, Adam Izdebski, Lee Mordechai, and Timothy Newfield. «Plagues, climate change, and the end of an empire: A response to Kyle Harper's The Fate of Rome (3): Disease, agency, and collapse». In: *History Compass* 16 (Nov. 2018). DOI: 10.1111/hic3.12507 (cit. on p. 1).

[3] Ross Ronald and Hudson Hilda P. «An application of the theory of probabilities to the study of a priori pathometry.—Part II and -Part III». In: *Proc. R. Soc. Lond. A93212–225, year = 1917* (). DOI: http://doi.org/10.1098/rspa.1917.0014 (cit. on pp. 1, 5).

[4] Alain Barrat, Marc Barthélemy, and Alessandro Vespignani. «Epidemic spreading in population networks». In: *Dynamical Processes on Complex Networks*. Cambridge University Press, 2008, pp. 180–215 (cit. on p. 1).

[5] Fredrik Liljeros, Christofer R. Edling, Luís A. Nunes Amaral, H. Eugene Stanley, and Yvonne Åberg. «The web of human sexual contacts». In: *Nature* 411.6840 (June 2001), pp. 907–908. ISSN: 1476-4687. DOI: 10.1038/35082140. URL: http://dx.doi.org/10.1038/35082140 (cit. on p. 1).

[6] Romualdo Pastor-Satorras and Alessandro Vespignani. «Epidemic Spreading in Scale-Free Networks». In: *Phys. Rev. Lett.* 86 (14 Apr. 2001), pp. 3200–3203. DOI: 10.1103/PhysRevLett.86.3200. URL: https://link.aps.org/doi/10.1103/PhysRevLett.86.3200 (cit. on p. 1).

[7] Lau JT, Yang X, Tsui HY, and Pang E. «SARS related preventive and risk behaviours practised by Hong Kong-mainland China cross border travellers during the outbreak of the SARS epidemic in Hong Kong.» In: *J Epidemiol Community Health.* (2004). DOI: 10.1136/jech.2003.017483 (cit. on p. 2).

[8] David P Durham and Elizabeth A Casman. «"Incorporating individual health-protective decisions into disease transmission models: a mathematical framework."» In: *Journal of the Royal Society, Interface vol. 9,68 (2012): 562-70.* (2012). DOI: 10.1098/rsif.2011.0325 (cit. on p. 2).

[9] Beutels P, Jia N, Zhou QY, Smith R, Cao WC, and de Vlas SJ. «The economic impact of SARS in Beijing, China.» In: *Trop Med Int Health. 2009;14 Suppl 1:85-91.* (2009). DOI: 10.1111/j.1365-3156.2008.02210.x (cit. on p. 2).

[10] G Rubin, Richard Amlôt, Lisa Page, and Simon Wessely. «Public Perceptions, Anxiety, and Behaviour Change in Relation to the Swine Flu Outbreak: Cross Sectional Telephone Survey». In: *BMJ (Clinical research ed.)* 339 (Feb. 2009), b2651. DOI: 10.1136/bmj.b2651 (cit. on p. 2).

[11] James Jones and Marcel Salathé. «Early Assessment of Anxiety and Behavioral Response to Novel Swine-Origin Influenza A(H1N1)». In: *PloS one* 4 (Dec. 2009), e8032. DOI: 10.1371/journal.pone.0008032 (cit. on p. 2).

[12] Daihai He, Jonathan Dushoff, Troy Day, Junling Ma, and David Earn. «Inferring the causes of the three waves of the 1918 influenza pandemic in England and Wales». In: *Proceedings. Biological sciences / The Royal Society* 280 (Sept. 2013), p. 20131345. DOI: 10.1098/rspb.2013.1345 (cit. on p. 2).

[13] Duo Yu, Qianying Lin, Alice Chiu, and Daihai He. «Effects of Reactive Social Distancing on the 1918 Influenza Pandemic». In: *PLoS ONE* 12 (July 2017). DOI: 10.1371/journal.pone.0180545 (cit. on p. 2).

[14] Tomas Philipson. «Private Vaccination and Public Health: An Empirical Examination for U.S. Measles». In: *Journal of Human Resources* 31.3 (1996), pp. 611–630. URL: https://ideas.repec.org/a/uwp/jhriss/v31y1996i3p611-630.html (cit. on p. 2).

[15] Abigail Harrison, Jennifer Smit, and Myers L. «Prevention of HIV/AIDS in South Africa: A review of behaviour change interventions, evidence and options for the future». In: *South African Journal of Science* 96 (June 2000), pp. 285–290 (cit. on p. 2).

[16] Avner Ahituv, V. Hotz, and Tomas Philipson. «The Responsiveness of the Demand for Condoms to the Local Prevalence of AIDS». In: *Journal of Human Resources* 31 (Sept. 1996), pp. 869–897. DOI: 10.2307/146150 (cit. on p. 2).

[17] Nicola Perra. «Non-pharmaceutical interventions during the COVID-19 pandemic: A review». In: *Physics Reports* 913 (Feb. 2021). DOI: 10.1016/j.physrep.2021.02.001 (cit. on p. 2).

[18] Holly Seale, Clare Dyer, Ikram Abdi, Kazi Rahman, Yanni Sun, Mohammed Qureshi, Alexander Dowell-Day, Jonathon Sward, and Md Saiful Islam. «Improving the impact of non-pharmaceutical interventions during COVID-19: Examining the factors that influence engagement and the impact on individuals». In: *BMC Infectious Diseases* 20 (Aug. 2020). DOI: 10.1186/s12879-020-05340-9 (cit. on p. 2).

[19] Seth Flaxman et al. *Estimating the number of infections and the impact of non-pharmaceutical interventions on COVID-19 in European countries: technical description update*. 2020. arXiv: 2004.11342 (cit. on p. 2).

[20] Benjamin Cowling et al. «Impact assessment of non-pharmaceutical interventions against coronavirus disease 2019 and influenza in Hong Kong: an observational study». In: *The Lancet Public Health* 5 (Apr. 2020). DOI: 10.1016/S2468-2667(20)30090-6 (cit. on p. 2).

[21] Juan Yang et al. «Despite vaccination, China needs non-pharmaceutical interventions to prevent widespread outbreaks of COVID-19 in 2021». In: *Nature Human Behaviour* 5.8 (Aug. 2021), pp. 1009–1020. DOI: 10.1038/s41562-021-01155-. URL: https://ideas.repec.org/a/nat/nathum/v5y2021i8d10.1038_s41562-021-01155-z.html (cit. on p. 2).

[22] N. Perra, B. Gonçalves, R. Pastor-Satorras, and A. Vespignani. «Activity driven modeling of time varying networks». In: *Scientific Reports* 2.1 (June 2012). ISSN: 2045-2322. DOI: 10.1038/srep00469. URL: http://dx.doi.org/10.1038/srep00469 (cit. on pp. 2, 10, 11).

[23] William Ogilvy Kermack and Anderson G McKendrick. «A contribution to the mathematical theory of epidemics». In: *Proceedings of the royal society of london. Series A, Containing papers of a mathematical and physical character* 115.772 (1927), pp. 700–721 (cit. on p. 5).

[24] Steven Abrams et al. «Modeling the early phase of the Belgian COVID-19 epidemic using a stochastic compartmental model and studying its implied future trajectories». In: (2021). DOI: 10.1101/2020.06.29.20142851 (cit. on p. 6).

[25] M. E. J. Newman. «The structure of scientific collaboration networks». In: *Proceedings of the National Academy of Sciences* 98.2 (2001), pp. 404–409. DOI: 10.1073/pnas.98.2.404. eprint: https://www.pnas.org/doi/pdf/10.1073/pnas.98.2.404. URL: https://www.pnas.org/doi/abs/10.1073/pnas.98.2.404 (cit. on p. 10).

[26] David Lazer et al. «Computational Social Science». In: *Science* 323.5915 (2009), pp. 721–723. DOI: 10.1126/science.1167742. eprint: https://www.science.org/doi/pdf/10.1126/science.1167742. URL: https://www.science.org/doi/abs/10.1126/science.1167742 (cit. on p. 10).

[27] Alain Barrat, Marc Barthélemy, and Alessandro Vespignani. «Epidemic spreading in population networks». In: *Dynamical Processes on Complex Networks*. Cambridge University Press, 2008, pp. 13–17 (cit. on p. 10).

[28] HW Hethcote and JA Yorke. «Springer Lecture Notes in Biomathematics». In: (1984) (cit. on p. 10).

[29] Nicolò Gozzi, Martina Scudeler, Daniela Paolotti, Andrea Baronchelli, and Nicola Perra. «Self-initiated behavioral change and disease resurgence on activity-driven networks». In: *Phys. Rev. E* 104 (1 July 2021), p. 014307. DOI: 10.1103/PhysRevE.104.014307. URL: https://link.aps.org/doi/10.1103/PhysRevE.104.014307 (cit. on pp. 19, 53).

[30] Stephen J.W. Evans and Nicholas P. Jewell. «Vaccine Effectiveness Studies in the Field». In: *New England Journal of Medicine* 385.7 (2021), pp. 650–651. DOI: 10.1056/NEJMe2110605 (cit. on p. 48).